The global structure of galactic discs

Grijs, R. de

Published in:
Monthly Notices of the Royal Astronomical Society

DOI:
10.1046/j.1365-8711.1998.01896.x

Publication date:
1998

1998

Mon. Not. R. Astron. Soc. **000**, 000–000 (1998)

The global structure of galactic discs

R. de Grijs[1,2]
[1] *Kapteyn Astronomical Institute, P.O. Box 800, 9700 AV Groningen, The Netherlands*
[2] *Astronomy Dept., University of Virginia, P.O. Box 3818, Charlottesville, VA 22903-0818, USA, grijs@virginia.edu (current address)*

Received date; accepted date

ABSTRACT
A statistical study of global galaxy parameters can help to improve our understanding of galaxy formation processes. In this paper we present the analysis of global galaxy parameters based on optical and near-infrared observations of a large sample of edge-on disc galaxies.
We found a correlation between the ratio of the radial to vertical scale parameter and galaxy type: galaxies become systematically thinner when going from S0's to Sc's, whereas the distribution seems to level off for later types.
The observed scale length ratios (and thus the radial colour gradients) largely represent the galaxies' dust content. On average the colour gradients indicated by the scale length ratios increase from type Sa to at least type Sc. For galaxy types later than Sc, the average colour gradient seems to decrease again.
The distribution of K-band (edge-on) disc central surface brightnesses is rather flat, although with a large scatter. However, the latest-type sample galaxies ($T > 6$) show an indication that their average disc central surface brightnesses may be fainter than those of the earlier types. This effect is probably not the result of dust extinction.

Key words: dust, extinction; galaxies: fundamental parameters; galaxies: photometry; galaxies: structure

1 A STATISTICAL ANALYSIS

A study of the statistical properties of highly inclined, or "edge-on" galaxies benefits greatly from the special orientation with respect to the line of sight of such galaxies. Observations of edge-on galaxies provide us with direct measurements of the luminosity and colour distributions both perpendicular to the galaxy planes and along the galaxies' major axes at various heights above the plane. Indirectly, these luminosity distributions can be related to the galaxies' density distributions and thus their global structure. Moreover, in-depth knowledge of the dust distribution, and hence the optical depth of galaxies, is important for our understanding of galaxy evolution.

1.1 The flattening of exponential discs

A major advantage of studying highly inclined galaxies is that one can determine their radial and vertical scale parameters directly and independently, since the dependence of these parameters on inclination is smallest for the highest inclinations (e.g., van der Kruit & Searle 1981a; de Grijs et al. 1997). These scale parameters provide us with information about the intrinsic shape of galaxy discs, i.e., their flattening, in a more direct way than the canonical axis ratios. Moreover, since the vertical scale height, $z_0 = 2h_z$ (where h_z is the exponential scale height), is to first order independent of radius (e.g., van der Kruit & Searle 1981a,b, 1982a; Kylafis & Bahcall 1987; Shaw & Gilmore 1990; Barnaby & Thronson, Jr. 1992; but see de Grijs & Peletier 1997), the radial to vertical scale parameter ratio, h_R/z_0, can often be determined more accurately than the major to minor axis ratio.

By studying the scale parameter ratio statistically, we may be able to put constraints on the disc formation processes as well as on the stability of galaxy discs (e.g., Bottema 1993). When considering the physical processes that determine the scale parameters one does not immediately expect a strong correlation between scale length and scale height. The scale height is likely determined by the internal, secular evolution of the stellar velocity dispersion (e.g., van der Kruit & Searle 1981a; Carlberg 1987), whereas the scale length is basically the result of the composition of the protogalaxy (Fall 1983; van der Kruit 1987).

However, one might expect that in a larger disc, with a greater rotation velocity, the heating of the disc stars may be more violent, thus resulting in a larger scale height. Therefore, one may expect a correlation between the rotation velocity (which can be related directly to the scale length) of a galaxy disc and the scale height, although the precise dependence is yet unknown (see, e.g., Bottema 1993).

Thus, statistics on the ratio of scale length to scale

height can be expected to give information on the importance of the formation processes in disc galaxies with different properties.

Moreover, once the h_R/z_0 ratio is known, one may be able to determine the (theoretical) maximum rotation of a disc from measurements of the vertical disc dispersion (Bottema 1993). Therefore, a statistical treatment of the scale parameter ratio may put general constraints on both the kinematical properties and the global stability of galaxy discs.

Bottema (1993) predicts that a constant value for the h_R/z_0 ratio leads to a more or less constant mass-to-light ratio of the old disc, $(M/L)_B$, under the assumption that we are dealing with exponential, locally isothermal discs with a constant ratio of vertical to radial velocity dispersion. On the other hand, if we assume a linear relationship between the old-disc absolute luminosity and the vertical velocity dispersion, Bottema (1993) shows that, for a constant $(M/L)_B$, the h_R/z_0 ratio decreases rapidly from faint galaxies to a constant level for normal and bright galaxies. Thus, in general, the observed velocity dispersions imply that a constant old-disc mass-to-light ratio results in an approximately constant scale parameter ratio, whereas a constant scale parameter ratio also leads to a mass-to-light ratio that is, to first order, constant.

In fact, these predictions imply that all galaxy discs are governed by equal mass-to-light ratios in the old stellar populations, assuming that all galaxy discs have approximately the same colour (Bottema 1993).

However, the assumption of a constant and equal mass-to-light ratio of the old-disc population in disc galaxies is probably not physically realistic, considering the range of colours observed within and among galaxies (e.g., de Jong 1996c, and references therein). Therefore, the predicted relationships should be treated with caution and only be used as general guidelines.

1.2 Colour gradients as diagnostics

Broad-band colours are relatively easy to obtain and are therefore the most widely used colour diagnostics to date. They immediately reveal the approximate nature of a galaxy, which is to first order determined by its dominant stellar population and dust content.

Although for the detailed analysis of galaxy luminosity and colour profiles one needs to adopt *a priori* assumptions concerning the evolutionary stellar population synthesis, the initial mass function, the metallicity and the star formation history, as well as about the dust geometry and its characteristics, de Jong (1996c) shows that the colours formed from different broad-band combinations correlate strongly, which indicates that these colours are probably caused by the same physical process. Therefore, broad-band colours can be used as indicators of changes in the gross properties of galaxies (e.g., changes in metallicity and/or dust contamination).

All systematic colour differences induced by stellar population changes and metallicity gradients are generally considerably smaller than the reddening due to dust, however.

1.2.1 Radial colour gradients in edge-on disc galaxies

In contrast to the large number of studies of radial colour gradients in moderately inclined and face-on spiral galaxies (e.g., de Jong 1996c, and references therein), the colour behaviour of highly inclined and edge-on galaxies has not received much attention. In highly inclined galaxies, the study and interpretation of intrinsic colour gradients is severely hampered by the presence of dust in the galaxy planes, which causes the dust lane to appear as a red feature in vertical colour profiles (e.g., Hamabe et al. 1979; Hegyi & Gerber 1979; van der Kruit & Searle 1981b; Jensen & Thuan 1982; de Grijs et al. 1997).

In individual edge-on galaxies, it is generally found that the colours along the major axes, i.e., the locations of the dust lanes, remain nearly constant (e.g., Sasaki 1987; Wainscoat et al. 1990; Aoki et al. 1991; Peletier & Balcells 1997), although in most cases the outermost disc regions tend to be slightly bluer on the major axis (e.g., Sasaki 1987), which may be explained in terms of an increasingly metal-poor population or a decreased amount of dust at larger galactocentric distances. Generally, as the height above the dust lane and its embedded young disc increases, the radial colour gradients become small or statistically insignificant (e.g., Hamabe et al. 1979, 1980; van der Kruit & Searle 1982a,b; Jensen & Thuan 1982; Peletier & Balcells 1997).

1.2.2 Colour gradients from scale length ratios

Since the dust influence varies as a function of passband, scale length ratios could be used as a diagnostic to estimate colour gradients and the dust content of a given galaxy.

Evans (1994) studied the effects of dust on the stellar scale length as a function of wavelength, under the assumption that the resulting scale length differences are solely due to dust absorption. His models predict that these differences are small, at least for face-on galaxies, on the order of the observational uncertainties, and even smaller for galaxies with a prominent bulge component. According to his models, if the scale height ratio between dust and stars is ~ 0.5 (Peletier & Willner 1992; Evans 1994), Evans' (1994) models exclude face-on galaxies with $h_B/h_H \approx 2$. On the other hand, larger ratios can be obtained if a galaxy is inclined with respect to the line of sight.

The measurement of blue to red scale length ratios alone will not unambiguously reveal the dust content of a given galaxy, because any deviation from unity can equally well be explained by an intrinsic colour gradient, especially for face-on galaxies (Byun et al. 1994).

2 SAMPLE SELECTION, OBSERVATIONS, AND DATA REDUCTION

To study the structural parameters of edge-on spiral galaxies we selected a statistically complete sample taken from the Surface Photometry Catalogue of the ESO-Uppsala Galaxies (ESO-LV; Lauberts & Valentijn 1989) with the following properties:

- their inclinations are greater than or equal to 87°;
- the angular blue diameters (D_{25}) are larger than $2.'2$;
- the galaxy types range from S0 to Sd, and

- they should be non-interacting.

The inclinations were determined following Guthrie (1992), assuming a true axial ratio $\log R_0 = 0.95$, corresponding to an intrinsic flattening $q_0 = (b/a)_0$ of 0.11. From this intrinsic flattening the inclinations i were derived by using Hubble's (1926) formula

$$\cos^2 i = (q^2 - q_0^2)/(1 - q_0^2), \quad (1)$$

where $q = b/a$ is the observed axis ratio.

Of the total sample of 93 southern edge-ons, an arbitrary subsample of 24 galaxies was observed in the near-infrared K' band in two observing runs of 4 and 3 nights, respectively. The selection of these 24 observed sample galaxies depended solely on the allocation of telescope time; the galaxies cover the southern sky rather uniformly.

By applying a $V/V_{\rm max}$ completeness test (e.g., Davies 1990; de Jong & van der Kruit 1994) we derived that the ESO-LV is statistically complete for diameter-limited samples with $D_{25}^B \geq 1.'0$. To check the completeness of our subsample, we calculated, based on a limiting diameter $D_{25}^B \geq 2.'2$, that $V/V_{\rm max} = 0.502 \pm 0.253$, which implies statistical completeness.

The near-infrared observations were obtained with the IRAC2B camera at the ESO/MPI 2.2m telescope of the European Southern Observatory (ESO) in Chile. The IRAC2B camera is equipped with a Rockwell 256×256 pixel NICMOS3 HgCdTe array. For both observing runs, in July 1994 and January 1995, we used the IRAC2B camera with Objective C, corresponding to a pixel size of $0.''491$ (40 μm) and a field of view of $125'' \times 125''$. The near-infrared array is linear to within 1% up to $\sim 18,000$ counts for exposure times > 1 sec (see, e.g., de Grijs 1997).

At both runs we used the K' filter available at ESO (central wavelength $\lambda_{\rm c} = 2.15\mu$m, bandpass $\Delta\lambda = 0.32\mu$m). We chose to observe in K' rather than in K band (with $\lambda_{\rm c} = 2.2\mu$m, and $\Delta\lambda = 0.40\mu$m), since the K' band is almost as little affected by dust as the K band, but has a lower sky background (Wainscoat & Cowie 1992).

We took sky images and object frames alternately, both with equal integration times (in sequences of 12 × 10s), and spatially separated by $\sim 5'$.

An overview of the near-infrared observations can be found in de Grijs et al. (1997).

The major part of the (supplementary and additional) optical B and I-band observations of our sample galaxies were obtained using the Danish 1.54m telescope at ESO, equipped with a 1081×1040 pixel TEK CCD with a pixel size of 24μm ($0.36\ ''$/pix). The field of view thus obtained is $6'.5 \times 6'.2$. The TEK CCD was used in slow read-out mode in order to decrease the pixel-to-pixel noise. The CCD used is linear to within 1% up to 44,000 counts and saturates at 65,536 counts.

Gaps in the observed sample were filled in by service observations with the Dutch 0.92m telescope at ESO, equipped with a 512×512 pixel TEK CCD. It has a pixel size of 27 μm ($0.44''$/pix), corresponding to a field of view of $3'.9 \times 3'.9$. The CCD is linear to within 1% over the full 16-bit dynamic range.

At both telescopes we used the standard Johnson B filter and the Thuan & Gunn (1976) I filter, which characteristics match those of a Johnson I filter (Buser 1978). Both telescopes were used in direct imaging mode, at prime focus. Details of the specific observations can be found in Table 1.

For all observed galaxies we determined the colour terms required for the calibration using standard stars (Table 2).

During the reduction of the near-infrared observations, each sky frame was compared with the two sky frames taken nearest in time in order to detect stars in the sky frames. These stars were filtered out by using a median filter and thus the resulting cleaned sky images are very similar to the actual sky contributions.

To circumvent the effects of bad pixels and to obtain accurate flatfielding we moved the object across the array between subsequent exposures. Therefore, for most galaxies mosaicing of either 4 or 8 image frames was required to obtain complete galaxy images. The mosaicing was done by using common stars in the frames to determine the exact spatial offsets. In the rare case that no common stars could be determined, we used the telescope offsets as our mosaicing offsets. The overlapping area was used to determine the adjustment of sky levels needed by means of a least squares fit.

Bad pixels and bad areas on the array were masked out and not considered during the entire reduction process. Only after mosaicing was finished, the areas that still did not contain any valid observations were interpolated by a 2-dimensional linear plane fit (see Peletier [1993] for a detailed description of the reduction method used).

The calibration of the near-IR observations was done by using the SAAO/ESO/ISO Faint Standard Stars (Carter & Meadows 1995). We used the corrections published by Wainscoat & Cowie (1992) to transform the K' measurements to the K band. The accuracy of the K'-band zero-point offsets we could reach was ~ 0.08 mag at both observing runs. The limiting factors here were flatfielding errors.

The optical images were reduced following standard reduction procedures (see de Grijs & van der Kruit 1996); for the calibration of these observations Landolt fields were used (Landolt 1992). The optical calibration could be done to an accuracy of $\sim 0.03 - 0.05$ mag, depending on the telescope and observing run.

Both our optical observations and the K'-band data were taken at photometric (parts of) nights.

2.1 Internal and external consistency checks

2.1.1 Internal consistency checks

To get an impression of the quality of our observations, we performed both internal and external consistency checks. We observed some of our sample galaxies more than once through the same filter either with the same telescope but on different nights, or with a different telescope during an other observing run. These observations provide us with an internal consistency check. Fig. 1 shows the difference between minor axis profiles observed in optical passbands on different nights or with a different telescope, with independent determinations of the calibration coefficients. The error estimates are based on the sky noise. Details of the specific observations that were used to determine the difference profiles of Fig. 1 are given in Table 3.

In Fig. 2 a comparison between near-infrared observa-

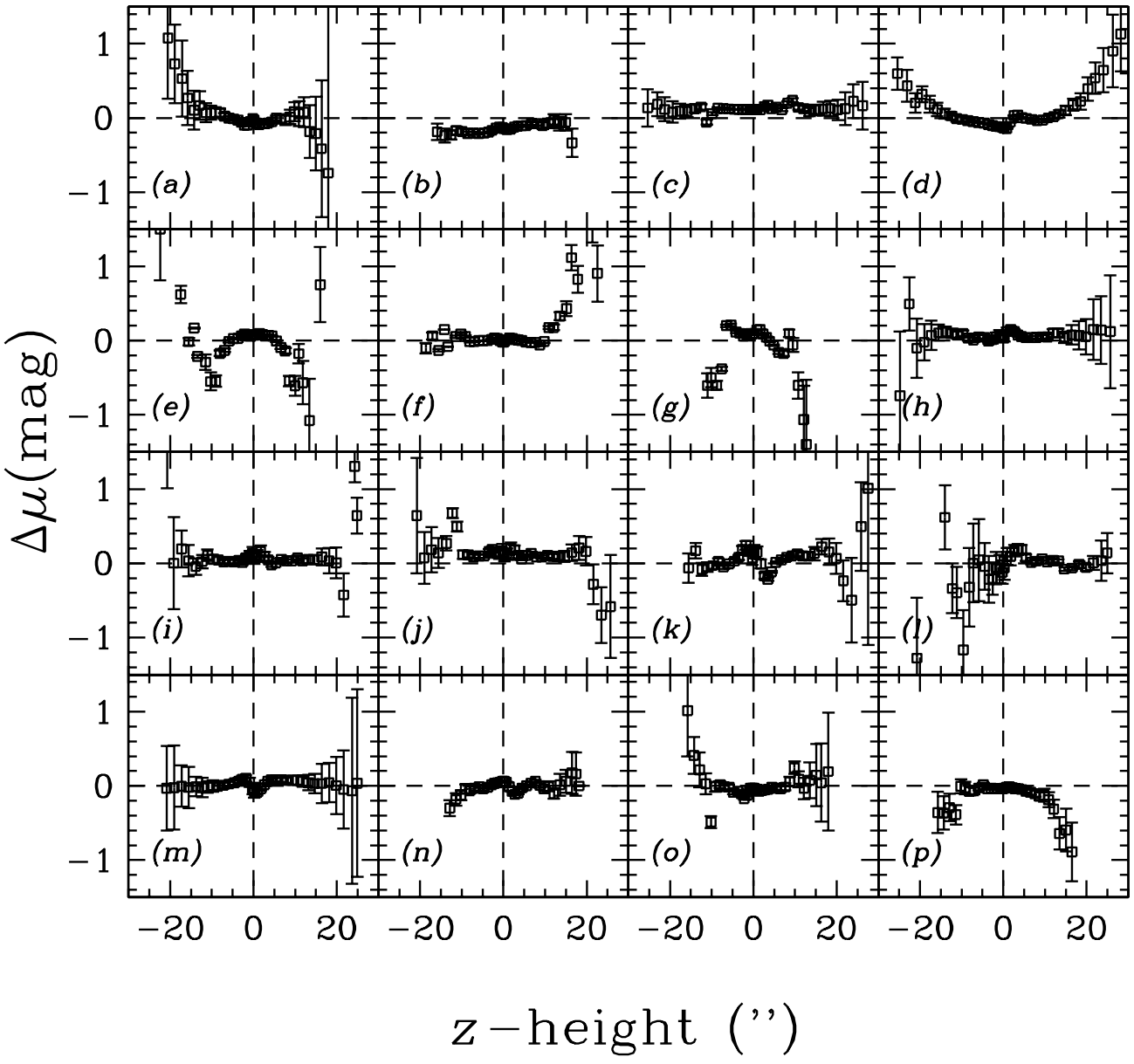

Figure 1. Comparison of the optical minor axis profiles obtained on different nights or with different telescopes. Details of the observations are given in Table 3

Table 1. Optical observations of the sample galaxies. Columns: (1) Galaxy name (ESO-LV); (2) Telescope used (Dan 1.5 = Danish 1.54m; Dut 0.9 = Dutch 0.92m); (3) Date of observation (ddmmyy) (4) Passband; (5) Exposure time (sec); (6) Seeing FWHM ($''$).

Galaxy (1)	Tel. (2)	Date (3)	Band (4)	Exp.time (5)	Seeing (6)
026-G06	Dan 1.5	090794	*B*	2×1800	2.1
	Dan 1.5	090794	*I*	2×900	1.6
033-G22	Dan 1.5	120194	*B*	2×1500	1.7
	Dan 1.5	120194	*I*	2×900	0.9
041-G09	Dan 1.5	100794	*B*	2×1800	1.7
	Dan 1.5	100794	*I*	2×900	1.4
074-G15	Dan 1.5	110794	*B*	2×1800	1.5
	Dan 1.5	110794	*I*	2×900	1.3
138-G14	Dan 1.5	080794	*B*	2×1800	2.2
	Dan 1.5	080794	*I*	2×900	1.6
141-G27	Dan 1.5	090794	*B*	2×1800	1.4
	Dan 1.5	090794	*I*	2×900	1.2
142-G24	Dan 1.5	110794	*B*	2×1800	1.2
	Dan 1.5	110794	*I*	2×900	1.4
157-G18	Dan 1.5	100194	*B*	2×1500	1.1
	Dan 1.5	100194	*I*	2×900	1.2
201-G22	Dan 1.5	090194	*B*	2×1500	1.3
	Dan 1.5	090194	*I*	2×900	1.2
202-G35	Dut 0.9	051094	*B*	2×1800	1.4
	Dut 0.9	061094	*I*	2×900	1.2
235-G53	Dan 1.5	110794	*B*	2×1800	1.4
	Dan 1.5	120794	*I*	600	1.5
	Dut 0.9	170396	*I*	1200	1.3
	Dut 0.9	210396	*I*	1200	1.3
240-G11	Dut 0.9	051094	*B*	2×1800	1.6
	Dut 0.9	061094	*B*	2×1800	1.6
	Dut 0.9	051094	*I*	2×1200	1.6
	Dut 0.9	061094	*I*	2×1200	1.6
263-G15	Dan 1.5	120194	*B*	2400	1.1
	Dan 1.5	090194	*I*	900	1.0
	Dan 1.5	100194	*I*	600	1.1
	Dan 1.5	120194	*I*	900	1.0
263-G18	Dut 0.9	100493	*B*	2400	1.7
	Dut 0.9	110493	*R*	720	1.3
	Dut 0.9	190194	*I*	2×900	1.2
269-G15	Dut 0.9	130493	*B*	2400	2.1
	Dut 0.9	130396	*I*	2×1200	1.3
286-G18	Dan 1.5	110794	*B*	2×1200	1.3
	Dan 1.5	090794	*I*	2×900	1.3
288-G25	Dut 0.9	051094	*B*	2×1800	1.3
	Dut 0.9	051094	*I*	2×1200	1.3
311-G12	Dan 1.5	120194	*B*	2×1500	1.0
	Dan 1.5	120194	*I*	2×900	1.0
315-G20	Dan 1.5	090194	*B*	2×1500	1.4
	Dan 1.5	090194	*I*	2×900	1.7
321-G10	Dut 0.9	280493	*B*	2400	1.3
	Dut 0.9	280493	*I*	300	1.2
322-G73	Dut 0.9	270493	*B*	2400	1.6
	Dut 0.9	230396	*I*	2×1200	1.2
322-G87	Dut 0.9	270493	*B*	2400	1.6
	Dut 0.9	270493	*I*	300	1.3
340-G08	Dan 1.5	100794	*B*	2×1800	1.6
	Dan 1.5	100794	*I*	2×900	1.3
340-G09	Dan 1.5	100794	*B*	2×1800	2.0
	Dut 0.9	140396	*I*	2×1200	1.4
358-G26	Dan 1.5	120194	*B*	2×1500	1.0
	Dan 1.5	120194	*I*	1200	1.0
358-G29	Dan 1.5	100194	*B*	2×1500	1.0
	Dan 1.5	100194	*I*	2×900	1.3

Table 1. (Continued)

Galaxy (1)	Tel. (2)	Date (3)	Band (4)	Exp.time (5)	Seeing (6)
377-G07	Dut 0.9	120493	*B*	2400	2.2
	Dut 0.9	100396	*I*	2×1200	1.2
383-G05	Dan 1.5	080794	*B*	2×1800	2.0
	Dan 1.5	080794	*I*	2×900	1.3
416-G25	Dan 1.5	130194	*B*	2×1500	1.2
	Dan 1.5	130194	*I*	2×900	1.0
435-G14	Dut 0.9	080493	*B*	2400	1.6
	Dut 0.9	201293	*B*	1000	1.7
	Dut 0.9	201293	*I*	2×900	1.0
435-G25	Dut 0.9	230493	*B*	5400	1.9
	Dut 0.9	231293	*B*	1800	1.8
	Dut 0.9	311293	*B*	1800	1.4
	Dut 0.9	050194	*B*	1800	1.5
	Dut 0.9	060194	*B*	1800	1.3
	Dut 0.9	230493	*I*	2×300	1.7
	Dut 0.9	231293	*I*	2×900	1.3
	Dut 0.9	060194	*I*	2×900	1.2
435-G50	Dan 1.5	100194	*B*	2×1500	1.2
	Dan 1.5	100194	*I*	2×900	1.1
437-G62	Dut 0.9	040195	*B*	2×1800	1.3
	Dut 0.9	040195	*I*	2×1200	1.0
444-G21	Dut 0.9	180493	*B*	2400	1.6
	Dut 0.9	230396	*I*	2×1200	1.2
446-G18	Dan 1.5	090794	*B*	2×1800	1.2
	Dan 1.5	090794	*I*	2×900	1.1
446-G44	Dan 1.5	110794	*B*	2×1800	1.1
	Dut 0.9	140396	*I*	2×1200	1.2
460-G31	Dan 1.5	080794	*B*	900	1.2
	Dan 1.5	100794	*B*	2700	1.3
	Dan 1.5	080794	*I*	2×900	1.5
487-G02	Dan 1.5	090194	*B*	2×1500	1.3
	Dan 1.5	090194	*I*	2×900	1.1
500-G24	Dan 1.5	130194	*B*	2×1500	1.2
	Dan 1.5	130194	*I*	2×900	1.0
505-G03	Dut 0.9	280493	*B*	2400	1.3
	Dut 0.9	010496	*I*	2×1200	1.3
506-G02	Dut 0.9	280493	*B*	2400	1.2
	Dut 0.9	280493	*I*	300	1.0
509-G19	Dan 1.5	100794	*B*	2×1800	1.3
	Dan 1.5	100794	*I*	2×900	1.0
531-G22	Dut 0.9	270994	*B*	2×1800	1.6
	Dut 0.9	270994	*I*	2×1200	1.5
555-G36	Dan 1.5	130194	*B*	2×1500	1.2
	Dan 1.5	130194	*I*	2×900	1.1
564-G27	Dut 0.9	211293	*B*	2400	1.4
	Dut 0.9	221293	*B*	1800	1.7
	Dut 0.9	211293	*I*	2×900	1.4
	Dut 0.9	221293	*I*	2×900	1.3

Table 2. Calibration transformation coefficients obtained for the different observing runs.

Pass-band (1)	zero point offset (2)	colour coeff. (3)	extinction (mag/airmass) (4)
April 1993, Dutch 0.92m telescope			
B	20.721 ± 0.109	0.110 ± 0.032	0.221 ± 0.030
I	20.606 ± 0.083	−0.037 ± 0.015	0.097 ± 0.030
December 1993/January 1994, Dutch 0.92m telescope			
B	20.982 ± 0.087	0.111 ± 0.027	0.242 ± 0.045
I	20.853 ± 0.048	−0.036 ± 0.013	0.104 ± 0.029
January 9–13, 1994, Danish 1.54m telescope			
B	22.331 ± 0.040	0.124 ± 0.031	0.105 ± 0.030
I	22.351 ± 0.040	−0.035 ± 0.022	0.021 ± 0.013
July 9–13, 1994, Danish 1.54m telescope			
B	22.984 ± 0.056	0.157 ± 0.006	0.308 ± 0.051
I	22.497 ± 0.028	−0.042 ± 0.018	0.030 ± 0.022
September/October 1994, Dutch 0.92m telescope			
B	21.232 ± 0.059	0.058 ± 0.027	0.210 ± 0.042
I	20.972 ± 0.048	−0.060 ± 0.018	0.064 ± 0.023
January 1995, Dutch 0.92m telescope			
B	20.900 ± 0.043	0.144 ± 0.030	0.242 ± 0.449
I	20.896 ± 0.017	−0.025 ± 0.015	0.065 ± 0.023
March 1996, Dutch 0.92m telescope			
I	20.928 ± 0.031	−0.037 ± 0.018	0.093 ± 0.032
July 9–12, 1994, ESO/MPI 2.2m telescope			
K	20.772 ± 0.088		0.002 ± 0.035
February 24–26, 1995, ESO/MPI 2.2m telescope			
K	20.697 ± 0.080		0.003 ± 0.029

NOTE:
[1]) Although the errors in the zero-point offsets quoted may be considerable, the errors obtained on the individual nights were significantly smaller. Therefore, the latter were used for the data reduction.

tions obtained on different nights is shown. We notice a significant difference between the individual observations of both ESO 263-G15 and ESO 446-G18 of up to 0.2 mag. This difference is likely due to the slightly varying response of the IRAC2B detector as a function of position across the array. The accuracy of the final, combined K' images is within the observational zero-point uncertainties, however.

The difference minor axis profiles in Figs. 1 and 2 show that in general the internal consistency is well within the zero-point and sky errors; the latter ones being generally of order 0.1–0.2 mag. In some cases differences in seeing show up in the central parts of the minor axis profiles as pronounced features in the difference profiles. We conclude that, although our observations are internally consistent, care has to be taken when interpreting the light at large distances from the galaxy planes, since at those distances the difference between individual observations can amount up to a few tenths of a magnitude. In a few cases, like for ESO 315-

Table 3. Details of the observations used for the internal consistency check of Fig. 1.
Columns: (1) Panel of Fig. 1; (2) Galaxy name (ESO-LV); (3) Passband; (4) and (5) Telescope used (Dan = Danish 1.54m; Dut = Dutch 0.92m) and date of observation (ddmmyy)

Figure (1)	Galaxy (ESO) (2)	Band (3)	Telescope/date (Profile 1) (4)	(Profile 2) (5)
(a)	235-G53	*I*	Dan 120794	Dut 170396
(b)	235-G53	*I*	Dut 170396	Dut 210396
(c)	240-G11	*B*	Dut 051094	Dut 061094
(d)	240-G11	*I*	Dut 051094	Dut 061094
(e)	263-G15	*I*	Dan 100194	Dan 110194
(f)	263-G15	*I*	Dan 100194	Dan 130194
(g)	435-G14	*B*	Dut 080493	Dut 201293
(h)	435-G25	*B*	Dut 230493	Dut 231293
(i)	435-G25	*B*	Dut 311293	Dut 050194
(j)	435-G25	*B*	Dut 311293	Dut 060194
(k)	435-G25	*B*	Dut 311293	Dut 230493
(l)	435-G25	*I*	Dut 230493	Dut 231293
(m)	435-G25	*I*	Dut 230493	Dut 060194
(n)	460-G31	*B*	Dan 090794	Dan 110794
(o)	564-G27	*B*	Dut 211293	Dut 221293
(p)	564-G27	*I*	Dut 211293	Dut 221293

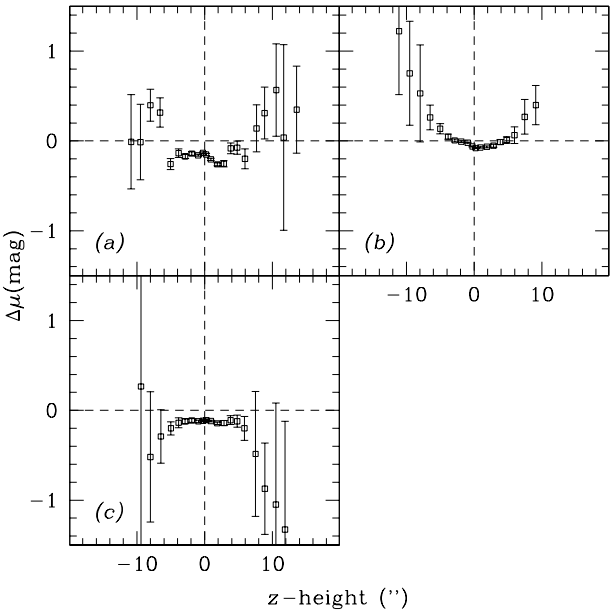

Figure 2. Comparison of near-infrared minor axis profiles obtained on different nights or with different telescopes. *(a)* K'-band observations of ESO 263-G15, observed on February 24 and 25, 1995; *(b)* Observations of ESO 286-G18 in K', observed on July 9 and 11, 1995; *(c)* K'-band observations of ESO 446-G18, obtained on July 9 and 12, 1995.

G20 and ESO 435-G14, the errors are large due to the low signal-to-noise ratio in either of the minor axis profiles used.

2.1.2 Comparison with published observations

Luminosity profiles of edge-on galaxies observed with modern detectors are scarcely available in the recent literature. For the galaxies in our present sample, a few individual measurements of optical luminosity profiles, either radially, vertically, or azimuthally averaged are available, although they are not sufficiently well documented to prove useful for a detailed comparison to our photometry. Fortunately, however, Mathewson et al. (1992) and Mathewson & Ford (1996), as well as Barteldrees & Dettmar (1994) have published detailed photometry of a significant fraction of our sample galaxies. From the detailed comparison of our photometry to theirs, as discussed in the following sections, our main conclusion is that, within the observational errors, we can reproduce the results published in the literature.

In de Grijs et al. (1997) we compared our observations of the large southern edge-on galaxy ESO 435-G25 in the near-infrared K band with those of Wainscoat et al. (1989). Although our observations of ESO 435-G25 are of a much higher quality and were taken with a much higher resolution, we find remarkably good agreement between Wainscoat et al.'s (1989) and our K-band observations.

2.1.2.1 Comparison with Mathewson et al. (1992) A large and homogeneous set of observations of southern Sb–Sc galaxies has been published recently by Mathewson et al. (1992) and Mathewson & Ford (1996), of which we used their azimuthally averaged luminosity profiles for a detailed comparison with our observations, see Fig. 3 of de Grijs et al. (1997). Unfortunately, since Mathewson et al. (1922) and Mathewson & Ford (1996) did not tabulate the ellipticities nor the position angles used for the individual ellipses obtained for each galaxy, we can at best compare azimuthally averaged profiles which were obtained with the same free parameters.

In general, we find that the differences between our and Mathewson's measurements are small, although clear deviations are appreciated in a number of cases. In particular for those galaxies for which the difference between our and Mathewson's profiles is relatively large, we used the individual observations to check our results.

2.1.2.2 Comparison with Barteldrees & Dettmar (1994) Barteldrees & Dettmar (1994) presented detailed optical surface photometry for a sample of 27 edge-on disc galaxies, which has 8 galaxies in common with our sample. The observations were done in the Thuan & Gunn (1976) g and r bands, for which the transformation to the Johnson B band is obtained as follows (Barteldrees & Dettmar 1994; Thuan & Gunn 1976):

$$g = B - 0.423(B-R) - 0.14 \tag{2}$$

and

$$r = B - 1.78(B-V) + 0.37 \tag{3}$$

We extracted surface brightness profiles along the galaxies' major axes, and compared these to the major axis profiles plotted by Barteldrees & Dettmar (1994). To do so, we calculated the transformations from the standard Johnson B band to Thuan & Gunn (1976) g and r band, using B–V and B–R colours taken from the ESO-LV. The resulting difference profiles are shown in Fig. 3. The close agreement resulting from this comparison leads us to the conclusion that our photometry reproduces that of Barteldrees & Dettmar (1994) to within the observational uncertainties.

3 APPROACH

3.1 Determination of the exponential scale length

Knapen & van der Kruit (1991), among others, have shown that the scale lengths of a particular galaxy, determined by different authors, may vary by $\approx 20\%$. The scale length determinations depend heavily on the radial fitting range, which is due to the fact that in general the radial profiles are not exactly exponential. Moreover, a patchy dust distribution in a particular galaxy can easily lead to varying estimates of the scale length, depending on the way the data is reduced (e.g., Giovanelli et al. 1994).

Since we wish to compare scale lengths determined in different passbands within and among galaxies, we need to choose the radial regions over which the disc exponential scale lengths are fitted in a consistent way.

The method that is generally used to determine the scale lengths of disc galaxies is by applying a bulge-disc decomposition algorithm to the azimuthally (elliptically) averaged radial luminosity profiles. However, when dealing with highly inclined or edge-on galaxies, the results from this technique start to be affected by the vertical as well as the radial luminosity components, which are characterised by significantly different scale parameters. Since the vertical scale height in a typical disc galaxy is generally an order of magnitude smaller than the radial scale length (see Sect. 4.1), the scale lengths derived from elliptically averaged luminosity profiles will be smaller than the true scale lengths.

Also, due to line-of-sight integration, the projection of a radially exponential disc will be a function of the form

$$L(R) = L_0(R/h_R)K_1(R/h_R) \tag{4}$$

(van der Kruit & Searle 1981a), where L_0 is the central surface luminosity, R the galactocentric distance, h_R the radial scale length, and K_1 the modified Bessel function of the first kind, which simplifies to

$$(R/h_R)K_1(R/h_R) = 1 + \frac{R^2}{2h_R^2}\ln(R/2h_R), \quad (R/h_R \ll 1); \tag{5}$$

$$(R/h_R)K_1(R/h_R) = \left(\frac{\pi R}{2h_R}\right)^{1/2}\exp(-R/h_R), \quad (R/h_R \gg 1). \tag{6}$$

in the limits. This means that the projected radial luminosity profile will be flattened towards the galaxy centre. Therefore, unless the projected scale lengths are obtained from the outer parts of the discs only, where $R/h_R \gg 1$, the resulting scale lengths will be estimated too large.

If a strong dust lane is present, the ellipse fitting is severely hampered by extinction effects that are hard to deal with numerically. It is generally assumed that the dust in

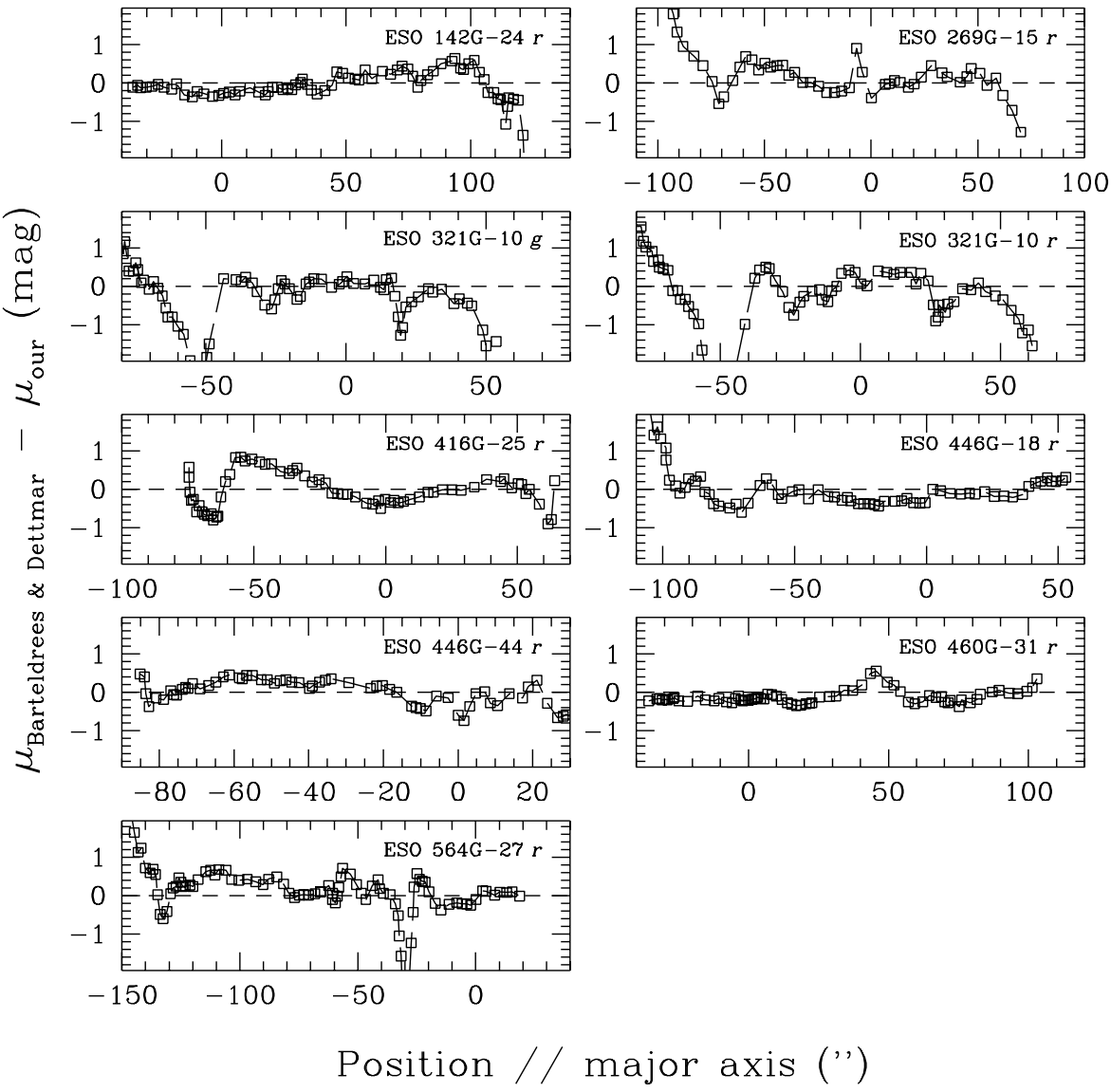

Figure 3. Comparison between major axis r (and g)-band profiles published by Barteldrees & Dettmar (1994), and those extracted from our observations. The width of our major axis profiles was chosen to be in the order of the seeing FWHM, since Barteldrees & Dettmar (1994) did not specify this.

a galaxy is, just like the stars, distributed in a disc with an exponentially decreasing density as a function of radius, although with a smaller scale height than that of the stellar component (e.g., Disney et al. 1989). Physically, this means that extinction plays a more prominent role near the galaxy centre than in the outer parts, thus resulting in an observed stellar scale length that is larger than the intrinsic scale length.

Although these effects counteract each other, the net result for a given galaxy depends on both the scale parameter ratio and the amount of dust, which both correlate with galaxy type (see, e.g., Sect. 4.1 and de Grijs et al. 1997). However, since the effects are not yet physically well understood, one should try to avoid using the scale lengths obtained from elliptically averaged luminosity profiles.

Alternatively, one can determine the scale lengths from luminosity profiles extracted at some distance from the galaxy planes and parallel to the galaxies' major axes. The main advantage of this method is that these profiles are less affected by dust than the elliptically averaged profiles. Moreover, if we assume that the disc thickness is constant to first order, as was argued in Sect. 1.1 (see also de Grijs & van der Kruit 1996; de Grijs & Peletier 1997), the intrinsic scale length obtained from the old-disc population at some distance from the plane will be essentially the same as the one at lower z distances. In the plane the situation becomes more complex due to the presence of a young stellar population. However, the young population is generally confined to the region very close to the plane, and likely has a scale height of only ~ 100pc (e.g., Hamabe & Wakamatsu 1989).

3.2 Determination of the exponential scale height

In the analysis of the vertical light distribution we distinguished between the different sides of the galaxy planes, to avoid possible dust contamination in the case of not perfectly edge-on orientations. In de Grijs & van der Kruit (1996) the basic reduction process was described in detail.

In de Grijs et al. (1997) we show that the vertical profiles are more peaked than expected for an isothermal distribution, and only marginally less peaked than exponential. The analysis shows that we can safely approximate the profile's shape with an exponential distribution at z heights greater than 1.5 scale heights. We fitted the vertical profiles out to 4 scale heights, thereby taking into account the possible presence of underlying thick disc components. Comparison for 24 galaxies with the I–K colour images in de Grijs et al. (1997) shows that in this vertical region the contamination of the stellar light by dust extinction can also be considered to be negligible.

Furthermore, in this vertical region the results obtained from the B and the I-band data do not differ significantly (de Grijs & Peletier 1997). Thus, in this region both the red and the blue light is dominated by the old-disc population, and the vertical luminosity profiles are not affected by, e.g., dust or the contribution of a young stellar population.

4 RESULTS

In Table 4 we present the B, I, and K-band scale lengths of our sample galaxies determined from luminosity profiles extracted at positions parallel to the major axes. To obtain these scale lengths, we applied a least-squares minimization algorithm to the luminosity profiles between 1 and 4 K-band radial scale lengths, unless indicated otherwise. The errors we quote are realistic rather than statistical in the sense that they represent the possible deviations from the mean if the radial fitting range is varied.

To obtain luminosity profiles representative of the light distributions parallel to the galaxies' major axes, we decided to extract them at those z distances, on the least dusty side of the planes, where the effects of dust extinction are greatly reduced. In choosing these distances we were limited by the signal-to-noise ratio in the K band. The best choice for the z distance to extract the profiles from turned out to be between 1.0 and 1.5 vertical scale heights. Although the influence of the central dust lane is greatly reduced at these distances from the planes, it is not (yet) completely negligible.

We used heliocentric velocities obtained by Mathewson et al. (1992) for the majority of our sample galaxies to base the calculation of our distance-dependent parameters on. The effects of the large-scale Hubble expansion were corrected for using Richter et al.'s (1987) formalism, which supposedly yields highly reliable values (Schmidt & Boller 1992).

As already touched upon in Sect. 3.1, since the effects that influence the determination of the scale lengths from elliptically averaged luminosity profiles of edge-on disc galaxies are not well understood, and may even be dependent on galaxy type, they should preferably not be used in an

Table 5. Extrapolated central surface brightnesses
All values were obtained using a radial fitting range between 1 and 4 K-band scale lengths, $h_{R,K}$ (I-band if no K-band data was available).

Galaxy	$\mu_{0,B}$	$\pm$	$\mu_{0,I}$	$\pm$	$\mu_{0,K}$	$\pm$
(ESO-LV)	(B, I, K mag arcsec^{-2})					
(1)	(2)	(3)	(4)	(5)	(6)	(7)
026-G06	22.16	0.15	20.11	0.14	17.54	0.10
033-G22	22.37	0.41	20.66	0.51	—	—
041-G09	22.28	0.22	19.44	0.10	16.45	0.05
074-G15	21.13	0.18	19.55	0.08	—	—
138-G14	20.70	0.10	19.51	0.07	18.34	0.52
141-G27	21.55	0.06	19.66	0.06	17.11	0.03
142-G24	20.42	0.09	19.12	0.17	17.37	0.12
157-G18	21.25	0.08	19.29	0.07	16.02	0.04
201-G22	19.36	0.67	18.28	0.11	—	—
202-G35	22.81	0.28	22.02	0.87	—	—
235-G53	21.64	0.13	19.16	0.42	—	—
240-G11	21.94	0.17	18.82	0.15	15.77	0.13
263-G15	22.08	0.23	19.49	0.24	—	—
263-G18	21.42	0.17	18.83	0.08	—	—
269-G15	21.54	0.17	19.33	0.11	16.34	0.14
286-G18	20.03	0.18	18.53	0.30	—	—
288-G25	20.14	0.10	18.04	0.04	15.53	0.19
311-G12	23.10	0.21	19.72	0.32	15.98	0.12
315-G20	19.92	0.18	18.51	0.36	—	—
321-G10	21.43	0.32	19.75	0.28	—	—
322-G73	21.44	0.45	18.95	0.45	—	—
322-G87	21.12	0.10	20.18	0.17	—	—
340-G08	20.34	0.43	21.45	0.17	19.19	0.59
340-G09	18.21	0.06	16.16	0.05	—	—
358-G26	19.13	0.19	17.36	0.22	15.66	0.36
358-G29	22.22	0.62	20.95	0.52	—	—
377-G07	22.60	0.13	19.92	0.12	16.24	0.10
383-G05	21.59	0.38	19.47	0.30	16.18	0.65
416-G25	20.65	0.09	18.44	0.08	15.84	0.26
435-G14	21.69	0.22	18.73	0.24	15.49	0.11
435-G25	20.51	0.05	19.73	0.05	—	—
435-G50	20.37	0.33	18.13	0.05	15.20	0.09
437-G62	20.86	0.39	20.57	0.26	—	—
444-G21	20.90	0.09	18.78	0.13	15.40	0.09
446-G18	20.96	0.09	18.74	0.05	15.79	0.03
446-G44	22.49	0.20	19.82	0.09	16.93	0.12
460-G31	20.53	0.06	18.64	0.07	15.83	0.12
487-G02	19.54	0.04	17.84	0.06	15.79	0.06
500-G24	20.58	0.08	19.39	0.18	—	—
505-G03	20.46	0.11	18.39	0.13	—	—
506-G02	21.59	0.09	18.83	0.07	15.61	0.04
509-G19	20.77	0.23	19.54	0.24	—	—
531-G22	21.73	0.11	20.54	0.15	—	—
555-G36	23.26	0.37	19.60	0.30	16.96	0.14
564-G27	21.34	0.11	20.29	0.13	—	—

Table 4. Scale parameters of the sample galaxies

Columns: (1) Galaxy name (ESO-LV); (2) and (3) I-band exponential scale height (the errors are of order $0.''03$); (4)–(7) B-band exponential scale length and measurement error; (8)–(11) I-band exponential scale length and measurement error; (12)–(15) K'-band exponential scale length and measurement error; (16); Maximum rotational velocity (Mathewson et al., 1992).

All values were obtained using a radial fitting range between 1 and 4 K-band scale lengths, $h_{R,K}$ (I-band if no K-band data was available).

Galaxy name	$h_{z,I}$		B band				I band				K band				$v_{\rm rot,max}$
			$h_{R,B}$	$\pm$	$h_{R,B}$	$\pm$	$h_{R,I}$	$\pm$	$h_{R,I}$	$\pm$	$h_{R,K}$	$\pm$	$h_{R,K}$	$\pm$	
(ESO)	($''$)	(h^{-1} kpc)	($''$)		(h^{-1} kpc)		($''$)		(h^{-1} kpc)		($''$)		(h^{-1} kpc)		(km s^{-1})
(1)	(2)	(3)	(4)	(5)	(6)	(7)	(8)	(9)	(10)	(11)	(12)	(13)	(14)	(15)	(16)
026-G06	3.40	0.38	31.84	4.70	3.58	0.53	26.21	2.94	2.95	0.33	18.69	2.05	2.10	0.23	100
033-G22[1]	2.45	0.47	40.52	3.42	7.72	0.65	22.12	1.23	4.21	0.23	—	—	—	—	113
041-G09	4.42	0.76	42.62	2.74	7.36	0.47	35.16	1.80	6.07	0.31	37.75	2.10	6.52	0.36	182
074-G15[2]	10.84	0.22	231.68	48.82	4.83	1.02	173.23	27.92	3.61	0.58	—	—	—	—	—
138-G14[2]	7.21	1.16	107.67	22.44	17.33	3.61	60.91	6.91	9.80	1.11	42.12	14.36	6.78	2.31	106
141-G27	4.16	0.29	49.87	5.00	3.51	0.35	37.42	3.01	2.63	0.21	25.98	4.87	1.83	0.34	87
142-G24	5.78	0.57	45.44	1.26	4.47	0.12	35.49	0.79	3.49	0.08	29.75	1.15	2.93	0.11	121
157-G18	5.01	0.33	49.22	2.29	3.20	0.15	38.53	0.99	2.50	0.06	36.19	1.78	2.35	0.12	91
201-G22	3.01	0.65	31.08	0.81	6.67	0.17	21.98	0.42	4.72	0.09	19.62	0.82	4.21	0.18	165
202-G35	3.44	0.26	24.40	2.44	1.81	0.18	21.22	1.08	1.57	0.08	—	—	—	—	116
235-G53	6.07	1.49	29.92	8.12	7.32	1.99	23.45	3.64	5.74	0.89	—	—	—	—	—
240-G11	3.77	0.62	67.87	4.24	11.15	0.70	41.34	1.57	6.79	0.26	—	—	—	—	241
263-G15	3.49	0.37	60.35	6.40	6.47	0.69	36.09	2.03	3.87	0.22	32.24	2.15	3.45	0.23	—
263-G18	2.95	0.56	32.85	2.56	6.21	0.48	24.27	1.59	4.59	0.30	—	—	—	—	—
269-G15	3.30	0.54	33.30	1.16	5.42	0.19	24.96	0.82	4.07	0.13	—	—	—	—	176
286-G18	3.65	1.67	20.19	0.76	9.21	0.35	17.55	0.46	8.01	0.21	15.57	0.69	7.10	0.31	323
288-G25[1]	3.46	0.41	19.18	0.37	2.28	0.04	17.70	0.34	2.10	0.04	—	—	—	—	—
311-G12	6.05	0.28	28.53	0.38	1.18	0.02	28.74	0.46	1.18	0.02	29.26	0.85	1.21	0.04	—
315-G20	4.01	0.88	22.67	2.48	4.99	0.55	19.36	1.30	4.26	0.29	18.16	5.52	4.00	1.21	—
321-G10	2.73	0.38	14.81	0.38	2.03	0.05	13.80	0.27	1.89	0.04	—	—	—	—	145
322-G73	5.01	1.22	16.65	0.98	2.87	0.17	11.59	0.70	1.99	0.12	—	—	—	—	—
322-G87	2.68	0.35	17.01	0.52	2.21	0.07	14.69	0.37	1.91	0.05	—	—	—	—	149
340-G08	2.23	0.32	18.06	0.48	2.63	0.07	13.40	0.23	1.95	0.03	—	—	—	—	99
340-G09	4.24	0.50	19.08	0.80	2.26	0.09	16.87	0.61	2.00	0.07	12.28	0.77	1.45	0.09	96
358-G26	6.19	0.46	12.84	0.20	0.95	0.01	13.10	0.20	0.97	0.01	—	—	—	—	—
358-G29[1]	6.95	0.56	12.64	0.30	1.02	0.02	12.88	0.32	1.04	0.03	14.73	0.90	1.19	0.07	160
377-G07	3.59	—	41.44	7.12	—	—	33.85	4.65	—	—	—	—	—	—	—
383-G05	8.85	1.46	36.78	3.17	6.06	0.52	28.18	1.39	4.65	0.23	21.36	1.09	3.52	0.18	—
416-G25[1]	3.47	0.96	12.94	0.66	3.59	0.18	11.28	0.49	3.13	0.13	8.82	0.21	2.45	0.06	209
435-G14	2.90	0.52	25.71	1.56	4.62	0.28	16.66	0.55	3.00	0.10	15.88	0.82	2.86	0.15	162
435-G25	4.98	0.57	88.08	4.63	10.16	0.53	51.25	2.17	5.91	0.25	44.09	1.76	5.09	0.20	201
435-G50	2.32	0.27	18.22	0.74	2.14	0.09	14.40	0.46	1.69	0.05	—	—	—	—	79
437-G62	5.31	0.66	30.42	1.67	3.77	0.21	25.77	0.84	3.20	0.10	21.52	0.64	2.67	0.08	—
444-G21	2.33	0.43	14.60	2.47	2.72	0.46	15.94	1.82	2.97	0.34	—	—	—	—	109
446-G18	2.27	0.55	22.38	0.64	5.38	0.15	16.60	0.36	3.99	0.09	14.27	0.43	3.43	0.10	190
446-G44	2.56	0.40	52.00	5.05	8.17	0.79	27.88	1.08	4.38	0.17	18.91	0.45	2.97	0.07	151
460-G31	3.74	0.97	38.36	4.72	9.95	1.22	26.26	1.92	6.81	0.50	19.01	1.35	4.93	0.35	225
487-G02[2]	4.71	0.48	24.09	0.42	2.44	0.04	21.66	0.39	2.19	0.04	22.92	0.57	2.32	0.06	154
500-G24	5.09	0.53	17.00	0.21	1.76	0.02	17.35	0.31	1.80	0.03	19.73	0.79	2.05	0.08	—
505-G03	3.14	0.20	55.78	8.44	3.52	0.53	37.46	3.79	2.36	0.24	—	—	—	—	89
506-G02	3.12	0.75	31.64	5.15	7.59	1.24	22.44	2.98	5.39	0.71	—	—	—	—	208
509-G19	3.64	1.86	23.03	1.88	11.74	0.96	17.39	1.14	8.86	0.58	18.52	2.07	9.44	1.06	—
531-G22	3.13	0.55	25.81	0.84	4.55	0.15	21.27	0.82	3.75	0.14	—	—	—	—	177
555-G36[2]	3.31	—	—	—	—	—	—	—	—	—	—	—	—	—	—
564-G27	3.26	0.46	67.07	5.21	9.43	0.73	37.96	1.08	5.34	0.15	40.59	1.85	5.71	0.26	162
575-G61	3.27	0.31	25.25	1.38	2.39	0.13	18.40	0.36	1.74	0.03	—	—	—	—	65

NOTES:

[1] These galaxies show an additional component, a "lens", with a luminosity profile in between the bulge and the disk component. The fits were applied to the following fitting ranges: ESO033-G22 — 2–4 $h_{R,I}$; ESO288-G25 – 2–6 $h_{R,I}$; ESO358-G29 and ESO416-G25 — 2–6 $h_{R,K}$.

[2] These galaxies are either greatly affected by foreground stars (ESO138-G14, fits between 2 and 4 $h_{R,K}$, and ESO555-G36), have a disk that cannot be approximated well by an exponential luminosity decline (ESO487-G02, fits between 1 and 3 $h_{R,K}$), or show a very irregular radial profile (ESO074-G15, fits between 0 and 2 $h_{R,I}$)

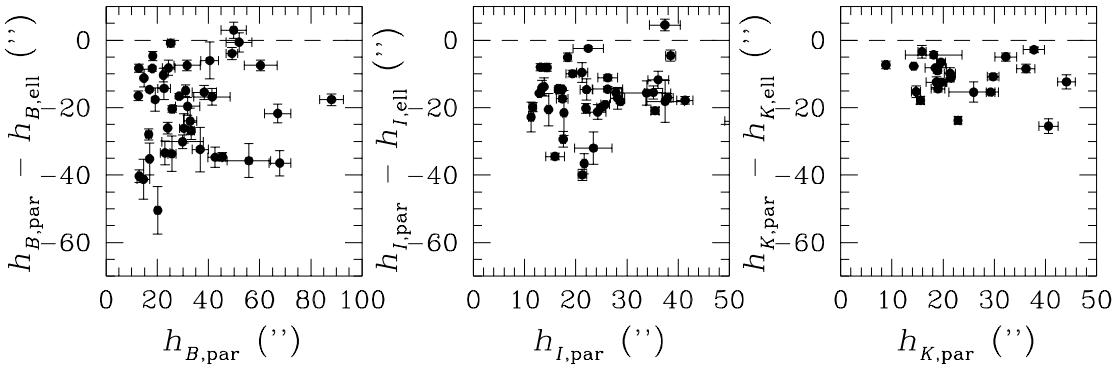

Figure 4. Comparison between the scale lengths determined using elliptically averaged luminosity profiles ($h_{<\mathrm{band}>,\mathrm{ell}}$) and profiles extracted parallel to the galaxies' major axes ($h_{<\mathrm{band}>,\mathrm{par}}$). The dashed lines indicate the locus of the data points if there were no difference between the two methods.

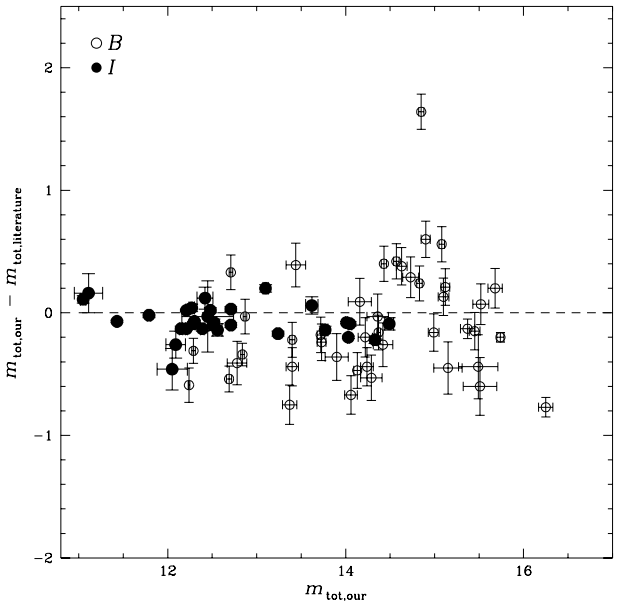

Figure 5. Comparison of our *B*- and *I*-band magnitudes to those published in the RC3 (*B* band) and by Mathewson et al. (1992, *I* band). The dashed line indicates the locus of equality.

analysis involving global scale parameters. To assess the importance of the effects discussed in Sect. 3.1, in Fig. 4 we compare the scale lengths derived from our sample galaxies using both methods. We notice clear systematic effects in all passbands, in the sense that the scale lengths obtained from the "elliptical" profiles are generally larger than those determined from the "parallel" profiles. The effect is smallest in the near-infrared, indicating that it is probably caused by dust contamination.

Although the ellipse fits should preferably not be used to derive scale parameters from the observed galaxy images, they are useful in providing estimates for the (edge-on) central surface brightnesses of galaxy discs. In Table 5 we tabulate the extrapolated edge-on disc central surface brightnesses.

The calibration of the observations was discussed in de Grijs et al. (1997). It was shown that our data agree sufficiently well in detail with those published previously. Here we present, in Table 6, the apparent magnitudes in the *B*, *I*, and *K* bands of the total galaxies as well as those of the disc components only. The apparent disc magnitudes are based on model discs obtained from ellipse fits to the outer galaxy isophotes.

In Fig. 5 we compare the (total) apparent *B* and *I*-band magnitudes with literature values; we took the apparent *B*-band magnitudes from de Vaucouleurs et al. (1991, RC3), and the apparent *I*-band magnitudes from the observations by Mathewson et al. (1992). Especially our determinations of the *I*-band apparent magnitudes agree rather well with those determined by Mathewson et al. (1992): the mean deviation between our and Mathewson et al.'s (1992) magnitude determinations is -0.07 ± 0.13 mag (based on a comparison of 30 galaxies); in the *B* band a larger scatter (of 0.45 mag, for 43 galaxies) between our and the RC3 determinations was found, although we do not detect a systematic difference between our apparent *B*-band magnitudes and the RC3 magnitudes (the mean deviation equals -0.09 mag).

In Table 6, we also present the absolute magnitudes in the *I* and *K* bands, M_I and M_K. We did not include the *B*-band absolute magnitudes, as those are too heavily affected by the internal dust extinction to be reliable.

4.1 Scale parameter ratios

Fig. 6 shows the dependence of the scale parameter ratio on galaxy type; we have also plotted the average scale parameter ratios per galaxy type. We notice a correlation between the h_R/z_0 ratio and revised Hubble type, in the sense that galaxies become systematically thinner when going from S0's to Sc's ($T = 5$), whereas the later types (Sd's, $T = 7$) seem to be at least as thin as the Sc's.

Although a correlation between the h_R/z_0 ratio and the rotation velocity was expected, based on the qualitative arguments presented in Sect. 1.1, we do not find any evidence for such a dependence (Fig. 7a), nor do we find any evi-

Table 6. Photometric characteristics of the sample galaxies
Columns: (1) Galaxy name (ESO-LV); (2)–(5), (6)–(9), (10)–(13) Apparent magnitudes of the total galaxy and the disk component only, and the 1σ observational errors, for the *B, I* and *K* bands (both determined in Chapter 6), respectively. The systematic errors due to variations in the photometric accuracy are of order 0.07 mag in *B*, 0.04 mag in *I*, and 0.08 mag in *K*; (14)–(16) Galactic extinction in the *B* band (taken from the RC3), the *I* and the *K* bands, respectively; (17)–(18) *I* and *K*-band absolute magnitudes, corrected for Galactic extinction (The *B*-band absolute magnitudes are generally heavily affected by dust extinction and have therefore not been included).

Galaxy	*B*-band magnitudes				*I*-band magnitudes				*K*-band magnitudes				$A_{G,B}$	$A_{G,I}$	$A_{G,K}$	M_I^0	M_K^0
(ESO)	total	±	disk	±	total	±	disk	±	total	±	disk	±			(*B, I, K* mag)		
(1)	(2)	(3)	(4)	(5)	(6)	(7)	(8)	(9)	(10)	(11)	(12)	(13)	(14)	(15)	(16)	(17)	(18)
026-G06	15.68	0.08	15.80	0.08	13.24	0.02	13.48	0.08	11.50	0.09	11.69	0.10	0.47	0.17	0.04	−18.76	−20.37
033-G22	15.37	0.08	15.51	0.03	14.03	0.01	14.33	0.06	—	—	—	—	0.43	0.16	0.04	−19.10	—
041-G09	13.52	0.01	13.52	0.01	12.21	0.01	12.21	0.03	—	—	—	—	0.62	0.23	0.05	−20.78	—
138-G14	14.85	0.03	15.20	0.05	14.01	0.01	14.37	0.03	—	—	—	—	0.60	0.22	0.05	−18.82	—
141-G27	14.57	0.03	14.57	0.03	12.71	0.02	12.83	0.04	10.57	0.12	10.57	0.12	0.21	0.08	0.02	−18.18	−20.26
142-G24	14.43	0.03	14.43	0.03	12.30	0.01	12.30	0.03	10.56	0.16	10.56	0.16	0.25	0.09	0.02	−19.33	−21.00
157-G18	13.72	0.04	13.72	0.04	12.29	0.02	12.29	0.02	9.79	0.50	9.79	0.50	0.00	0.00	0.00	−18.35	−20.85
201-G22	14.06	0.07	14.06	0.07	13.10	0.03	13.10	0.05	10.34	0.16	10.34	0.16	0.00	0.00	0.00	−20.13	−22.89
202-G35	12.71	0.02	12.71	0.02	11.79	0.02	11.79	0.04	—	—	—	—	0.00	0.00	0.00	−19.13	—
235-G53	14.37	0.02	15.46	0.06	12.45	0.01	13.19	0.04	—	—	—	—	0.09	0.03	0.01	−21.10	—
240-G11	13.44	0.11	13.66	0.11	11.11	0.16	11.50	0.06	—	—	—	—	0.04	0.01	0.00	−21.55	—
263-G15	14.22	0.08	14.22	0.08	11.19	0.01	11.19	0.01	9.09	0.15	9.09	0.15	1.24	0.45	0.11	−20.98	−22.74
263-G18	14.29	0.12	14.33	0.12	11.70	0.02	13.22	0.11	—	—	—	—	0.62	0.23	0.05	−21.49	—
269-G15	14.16	0.13	14.16	0.13	12.15	0.02	12.15	0.04	—	—	—	—	0.47	0.17	0.04	−20.65	—
286-G18	14.90	0.05	14.90	0.05	12.21	0.01	12.21	0.03	10.45	0.38	10.45	0.38	0.07	0.03	0.01	−22.69	−24.43
288-G25	13.73	0.05	13.73	0.05	11.62	0.01	11.62	0.03	—	—	—	—	0.00	0.00	0.00	−20.33	—
311-G12	12.24	0.01	13.32	0.03	10.04	0.01	10.85	0.03	7.35	0.20	8.36	0.61	1.49	0.54	0.13	−20.15	−22.43
315-G20	16.25	0.08	17.56	0.40	12.62	0.01	13.76	0.07	9.19	0.78	11.03	0.98	0.00	0.00	0.00	−20.67	−24.10
321-G10	13.90	0.13	14.84	0.07	12.05	0.17	12.05	0.15	—	—	—	—	0.35	0.13	0.03	−20.34	—
322-G73	13.37	0.08	13.68	0.09	11.84	0.02	12.26	0.02	—	—	—	—	0.52	0.19	0.04	−21.10	—
322-G87	14.24	0.07	14.24	0.07	12.09	0.11	12.09	0.11	—	—	—	—	0.49	0.18	0.04	−20.23	—
340-G08	15.52	0.09	16.22	0.04	13.77	0.03	13.95	0.04	—	—	—	—	0.16	0.06	0.01	−18.68	—
340-G09	15.08	0.03	15.08	0.03	13.62	0.07	13.62	0.07	11.34	0.63	11.34	0.63	0.20	0.07	0.02	−18.39	−20.62
358-G26	12.87	0.02	13.11	0.02	11.68	0.01	12.84	0.04	—	—	—	—	0.00	0.00	0.00	−19.23	—
358-G29	12.29	0.02	13.14	0.04	10.37	0.01	11.08	0.04	8.26	0.29	9.16	0.74	0.00	0.00	0.00	−20.73	−22.84
377-G07	15.49	0.22	15.49	0.22	13.49	0.07	13.49	0.09	—	—	—	—	0.34	0.12	0.03	—	—
383-G05	14.63	0.06	14.87	0.08	11.94	0.02	12.62	0.05	8.95	1.15	9.72	0.24	0.16	0.06	0.01	−20.78	−23.72
416-G25	14.42	0.11	14.65	0.04	12.52	0.03	12.81	0.05	10.35	0.76	11.38	1.12	0.03	0.01	0.00	−21.28	−23.44
435-G14	14.73	0.09	14.73	0.09	12.56	0.05	12.56	0.08	10.12	0.37	10.12	0.37	0.18	0.07	0.02	−20.36	−22.75
435-G25	12.78	0.11	13.23	0.14	11.05	0.03	11.54	0.07	8.42	0.41	8.63	0.52	0.25	0.09	0.02	−20.92	−23.48
435-G50	15.74	0.04	15.74	0.04	14.33	0.03	14.33	0.05	—	—	—	—	0.29	0.11	0.02	−17.70	—
437-G62	12.69	0.03	13.47	0.07	10.72	0.01	11.28	0.03	8.34	0.19	8.65	0.11	0.31	0.11	0.03	−21.43	−23.73
444-G21	15.15	0.16	15.15	0.16	14.05	0.02	14.05	0.03	—	—	—	—	0.25	0.09	0.02	−18.96	—
446-G18	15.12	0.05	15.32	0.06	12.71	0.02	13.21	0.04	10.17	0.42	10.84	0.42	0.22	0.08	0.02	−20.85	−23.33
446-G44	14.83	0.03	14.83	0.03	12.51	0.04	12.51	0.06	10.23	0.66	10.23	0.66	0.29	0.11	0.02	−20.15	−22.34
460-G31	14.99	0.06	15.39	0.09	12.48	0.02	13.28	0.03	10.02	0.56	10.55	0.60	0.71	0.26	0.06	−21.42	−23.68
487-G02	13.40	0.03	13.66	0.04	11.43	0.01	11.49	0.03	8.84	0.39	9.05	0.82	0.04	0.01	0.00	−20.18	−22.76
500-G24	12.84	0.02	13.25	0.03	10.92	0.01	11.31	0.03	—	—	—	—	0.34	0.12	0.03	−20.85	—
505-G03	13.40	0.07	13.40	0.07	12.39	0.02	12.39	0.04	—	—	—	—	0.25	0.09	0.02	−18.27	—
506-G02	14.13	0.04	14.37	0.27	12.45	0.29	13.06	0.11	—	—	—	—	0.46	0.17	0.04	−21.19	—
509-G19	15.10	0.06	15.10	0.06	12.32	0.01	12.32	0.04	9.58	0.44	9.58	0.44	0.21	0.08	0.02	−22.87	−25.55
531-G22	13.96	0.08	13.96	0.08	12.27	0.03	12.27	0.06	—	—	—	—	0.10	0.04	0.01	−20.58	—
555-G36	15.45	0.06	15.45	0.06	14.18	0.03	14.18	0.06	—	—	—	—	0.47	0.17	0.04	—	—
564-G27	14.36	0.12	14.56	0.12	12.42	0.09	13.02	0.11	9.72	0.34	9.72	0.34	0.56	0.20	0.05	−20.09	−22.64
575-G61	15.51	0.19	15.51	0.19	14.49	0.05	14.49	0.08	—	—	—	—	0.25	0.09	0.02	−17.05	—

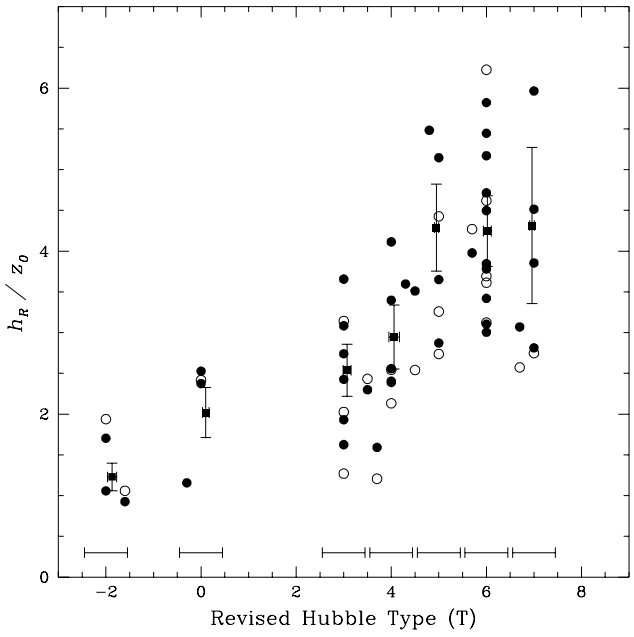

Figure 6. Dependence of the h_R/z_0 ratio on galaxy type for both I-band data (filled dots) and K-band observations (open circles). The filled squares show the I-band ratios averaged over the type bins indicated by the horizontal bars; the errors indicate the standard deviations of the distribution.

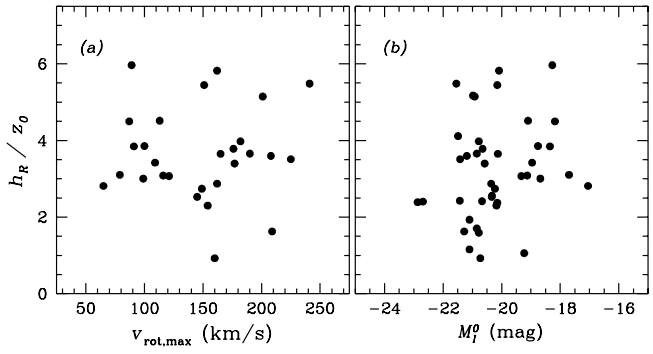

Figure 7. I-band scale parameters versus *(a)* the maximum rotation velocity, and *(b)* the absolute I-band magnitudes.

dence for a relationship between the h_R/z_0 ratio and the absolute magnitudes (Fig. 7b). In other words, the theoretical prediction that the scale parameter should decrease rapidly from faint galaxies to a constant level for normal and bright galaxies (Bottema 1993) could not be confirmed observationally. This implies that either the relationship is weak, i.e., smaller than the observational scatter, or the underlying assumptions (of, e.g., a constant $(M/L)_B$, and a linear relationship between the old-disc absolute magnitude and the disc vertical velocity dispersion) either have a large intrinsic scatter themselves or are not valid.

Table 7. Scale length ratios of the sample galaxies
Columns: (1) Scale length ratio; (2) (Sub)sample used; (4) Number of galaxies in the (sub)sample; (5) Resulting scale length ratio and standard deviation.

Gradient	Galaxy types	Number of Galaxies	Mean Ratio
(1)	(2)	(3)	(4)
h_B/h_I	$T > 2$	40	1.36 ± 0.22
	All types	45	1.32 ± 0.24
h_B/h_K	$T > 2$	22	1.65 ± 0.41
	All types	25	1.56 ± 0.46
h_I/h_K	$T > 2$	22	1.19 ± 0.17
	All types	25	1.15 ± 0.19

4.2 Radial colour gradients

As we argued in Sect. 1.2.2, one can study radial colour gradients within galaxies by comparing scale lengths determined in different passbands. In Fig. 8 we show the scale length ratios (indicating radial colour gradients) obtained for our sample galaxies.

In Table 7 we present the mean scale length ratios, both for our total sample and for the galaxies of type $T > 2$.

The main conclusion that we draw in de Grijs et al. (1997), based on the "elliptical" I versus K-band scale length ratios, still holds firmly, namely that on average the colour gradients indicated by the scale length ratios increase from type Sb ($T = 3$) to at least type Scd ($T = 6$), as is best seen in Figs. 8a and b. For galaxy types later than Scd, the colour gradients seem to become smaller again, although – due to small-number statistics – we cannot draw any firm conclusions in that range of galaxy types.

For the earliest-type sample galaxies ($T < 2$) we find very small colour gradients at these z distances. It is, in fact, expected that the intrinsic colour gradients at these heights above the planes are smaller than those in the planes, where the young population contributes to the luminosity. At these z heights we are looking at the old-disc population, which is very uniform in colour, as was argued in Sect. 1.2.1.

The results presented in this section are consistent with those published previously (e.g., Elmegreen & Elmegreen 1984; Peletier et al. 1994, 1995a; de Jong 1996a; and others), as will be shown in Sect. 5.3.

4.3 Correlations between gross galaxy properties

Since the sample we are dealing with is a diameter-selected sample of edge-on disc galaxies, a correction has to be applied to the observed parameters to represent a volume-limited sample (e.g., Davies 1990). Because the sample galaxies were selected to have a minimum blue major axis diameter at 25 B-mag arcsec^{-2}, D_{25}^B, of 2.′2, we have created a selection bias against low surface brightness galaxies and galaxies with small scale lengths. The main implications of such a selection bias have been discussed by de Jong (1996b). In Fig. 9 we show the implications of our selection bias with respect to the disc properties of the observed sample galaxies in the (h_R, μ_0) plane.

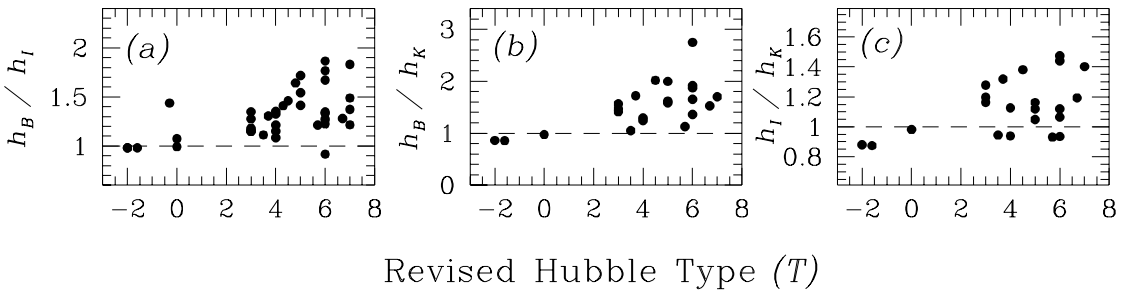

Figure 8. Scale length ratios as a function of revised Hubble type derived from the profiles extracted parallel to the galaxies' major axes. The dashed lines indicate the locus of galaxies which do not show any scale length difference between passbands.

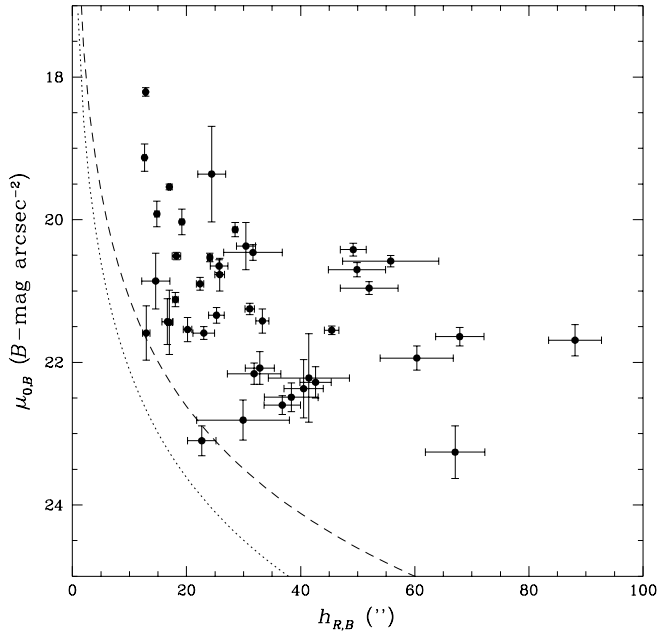

Figure 9. Illustration of the effects of sample selection based on a diameter limit. The dashed line represents a diameter-selection limit (of 2.′2) at 25 B-mag arcsec^{-2}; the dotted line is the limit for a diameter-selection limit at 26 B-mag arcsec^{-2}.

The dashed and dotted lines in this figure represent the selection limits for a limiting diameter of 2.′2, using the 25 and 26 B-mag arcsec^{-2} isophotes, for comparison. The diameter-selection criterion used implies that our sample should only contain galaxies to the right of the selection limit in Fig. 9.

Although our sample selection was based on the $D_{\rm orig}$ diameter tabulated in the ESO-LV catalogue, this diameter was not determined at exactly the 25 B-mag arcsec^{-2} isophote (ESO-LV), but varies with galaxy type. For spiral galaxies the diameters correspond to approximately 26 B-mag arcsec^{-2} isophotes; for earlier types the corresponding isophotes are in the range from 25.0–25.6 B-mag arcsec^{-2}.

As de Jong (1996b) remarks, since the number of galaxies in the sample will decrease as h_R^3 if all galaxies have the same scale length, it is not surprising that our sample does not contain galaxies with central B-band surface brightnesses fainter than about 23 B-mag arcsec^{-2}.

4.3.1 Type dependences

In Fig. 10 we show the distributions of global K-band galaxy parameters as a function of Hubble type. We did not apply an inclination correction to the galaxy parameters, but since we are dealing with edge-on galaxies, inclination *differences* do not play a significant role.

The distribution of (edge-on) K-band disc central surface brightnesses is rather flat (Fig. 10a), although with a large scatter. However, the latest-type sample galaxies ($T \geq 6$) show an indication that their disc central surface brightnesses may be fainter than those of the earlier types. Most likely, this effect is not the result of dust extinction, since the latest-type galaxies are not likely to contain more dust than the earlier and intermediate types, as was argued in Sect. 4.2. These results are consistent with those of de Jong (1996b).

Fig. 10b shows the distribution of the radial scale lengths of the galaxy discs, in kpc; we do not notice any clear correlation with galaxy type, apart from the observation that the earliest-type sample galaxies apparently have the smallest scale lengths, with only a small range of possible scale lengths compared to the range in the scale length distribution for galaxies of type $T > 2$. De Jong (1996b) noticed a possible lack of late-type galaxies with small scale lengths for his sample of 86 face-on disc galaxies, but remarked that this could be a selection effect. In fact, small galaxies (i.e., galaxies with small scale lengths) will have a greater possibility to be selected in a sample of edge-on galaxies than in a face-on galaxy sample, due to the line-of-sight integration through the galaxy discs. Therefore, his explanation seems to be valid, since we do not detect any lack of late-type disc galaxies with small scale lengths in our sample.

Finally, Fig. 10c shows the distribution of absolute I and K-band magnitudes with Hubble type. Since in edge-on disc galaxies the luminosity is, at least for the later-type galaxies ($T > 2$), dominated by the disc luminosity, and thus the relation between the disc and the total absolute magnitude is approximately linear, we could have deduced the distribution of absolute magnitudes from Figs. 10a and b (de Jong 1996b):

$$M_{\rm abs} \approx M_{\rm disc} \propto \mu_0 - 2.5\log(2\pi h_R^2), \qquad (7)$$

where μ_0 is the (edge-on) disc central surface brightness, and $M_{\rm abs}$ and $M_{\rm disc}$ are the absolute magnitudes of the total galaxy and the disc component only, respectively.

Because the scale length distribution of Fig. 10b does not show any dependence on type, the distribution of absolute magnitudes reflects the distribution of central surface brightnesses with type, again consistent with de Jong (1996b).

4.3.2 Dust

The distribution of galaxy colours as a function of Hubble type (corrected for Galactic foreground extinction) is shown in Figs. 11a–c for the $(B–I)_0$, $(B–K)_0$, and $(I–K)_0$ colours, respectively. We show the central disc colours, derived from the extrapolated central surface brightnesses, the colours of the total galaxy and those of the disc, denoted by different symbols. It is clear, that these colours follow the same distributions, although the scatter is large. In particular for the $(B–K)_0$ and $(I–K)_0$ colour distributions the colours derived from the total apparent magnitudes are systematically redder than the other two colour distributions. This is caused by dust, because the disc apparent magnitudes and the central surface brightnesses were obtained from ellipse fits to the outer disc regions, where the amount of dust is significantly lower than in the central plane. De Jong (1996b) notices a clear correlation between the colours of his 86 face-on spiral galaxies and galaxy type (but with a large scatter), whereas we do not find any such correlation. However, since our sample galaxies are heavily contaminated by dust, such a correlation, if intrinsic to the galaxies, may well be hidden by the interstellar dust.

In Figs. 11d–f we present colour-colour diagrams for our sample galaxies, for the colours described above. Although the distributions follow each other closely and the correlations are generally tight, the correlation between total galaxy colours is systematically offset, again due to dust. This evidence is supported by the very red $(B–K)_0$ colours of most of our galaxies, which are redder than those of bright giant ellipticals (with $B-K \sim 4.3$ [Peletier et al. 1994, 1995a]).

Therefore, Fig. 11 is completely dominated by dust effects; intrinsic colour gradients in the discs of galaxies, due to either metallicity or age gradients are too small to be observable, see also Sect. 5.3.

5 DISCUSSION

5.1 Main observational results

From the statistical analysis of the global structure parameters of our sample of edge-on disc galaxies in the *B, I,* and *K* bands, in this paper we present the following main observational results:

- We found a correlation between the h_R/z_0 ratio and the revised Hubble type (Fig. 6a), in the sense that galaxies become systematically thinner when going from S0's to Sc's, whereas the later types (later than Sc) seem to be at least as thin as the Sc's.
- On average the colour gradients indicated by the scale length ratios increase from type Sa to at least type Scd. For galaxy types later than Scd, the colour gradients seem to become smaller again.
- The distribution of (edge-on) *K*-band disc central surface brightnesses is rather flat, although with a large scatter. However, the latest-type sample galaxies ($T > 6$) show an indication that their disc central surface brightnesses may be fainter than those of the earlier types. Most likely, this effect is not the result of dust extinction.
- We do not find a clear correlation between galaxy type and integrated, disc, or central colours. The scatter in the distributions is probably caused by dust.

5.2 Kinematic constraints from structure analysis

As was discussed in Sect. 1.1, once the h_R/z_0 ratio is known, one may be able to determine the maximum rotation of a disc from measurements of the vertical disc dispersion, although the theoretical predictions are based on assumptions that show large intrinsic scatter themselves. Van der Kruit & Searle (1982a) found a mean scale parameter ratio of $h_R/z_0 = 5.0 \pm 1.8$ for their sample of 8 edge-on disc galaxies (predominantly later-type spirals) in the optical *J* band, whereas de Grijs & van der Kruit (1996) reported a mean ratio of $h_R/z_0 = 5.9 \pm 0.4$ based on the *I*-band characteristic length scales in their sample of 7 edge-on disc galaxies. These ratios are larger than the mean ratio found in this paper ($\langle h_R/z_0 \rangle = 3.7 \pm 1.3$).

To fit the observations of the maximum rotational velocity of disc-dominated Sc galaxies, h_R/z_0 needs to be of order 10 (Bottema 1993). The discrepancy between the observational results and the theoretical prediction leads Bottema (1993) to the conclusion that, for realistic h_R/z_0 ratios, the stellar velocity dispersions only allow the disc to have a (theoretical) maximum rotation of on average $(63 \pm 10)\%$ of the observed maximum rotation. This is significantly less than implied by results of the so-called maximum disc fits (e.g., van Albada & Sancisi 1986) that are widely used to model galaxy rotation curves, which predict a maximum-disc rotation of 85-90% of the observed rotation (Bottema 1993).

Recent estimates of the scale parameters of our Galaxy (e.g., Kent et al. 1991; see Sackett [1997] for an overview), yield a scale parameter ratio of $(h_R/z_0)_{\rm Gal} = 5.3 \pm 0.5$, which is consistent with the ratios published previously as well as with the data for external galaxies presented in this paper. However, although this ratio for our Galaxy is significantly less than the value of order 10 required theoretically (Bottema 1993), Sackett (1997) argues that new structural and kinematical constraints are consistent with a Galactic maximum disc with reasonable mass-to-light ratio, of $2 \leq M/L_V \leq 7$.

In Sect. 4.1 we showed that the h_R/z_0 ratio of our sample galaxies correlates with revised Hubble type. This effect is not likely to be caused by the presence of a thick disc in our earlier-type sample galaxies, since we used the thin disc scale parameters to derive the correlation (see also de Grijs & Peletier 1997). Part of the effect may be due to the distribution of the scale lengths among our sample galaxies, in the sense that the earlier-type galaxies tend to have smaller scale lengths. Moreover, van der Kruit & Searle (1982a) ar-

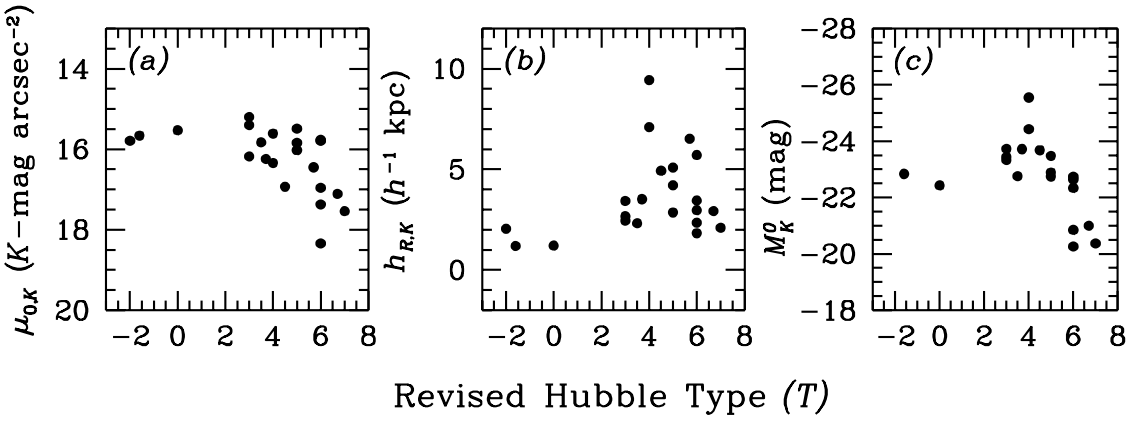

Figure 10. Distribution of global K-band galaxy properties as a function of galaxy type: *(a)* Central disc surface brightnesses; *(b)* disc radial scale lengths (in h^{-1} kpc); *(c)* Absolute magnitudes of the sample galaxies.

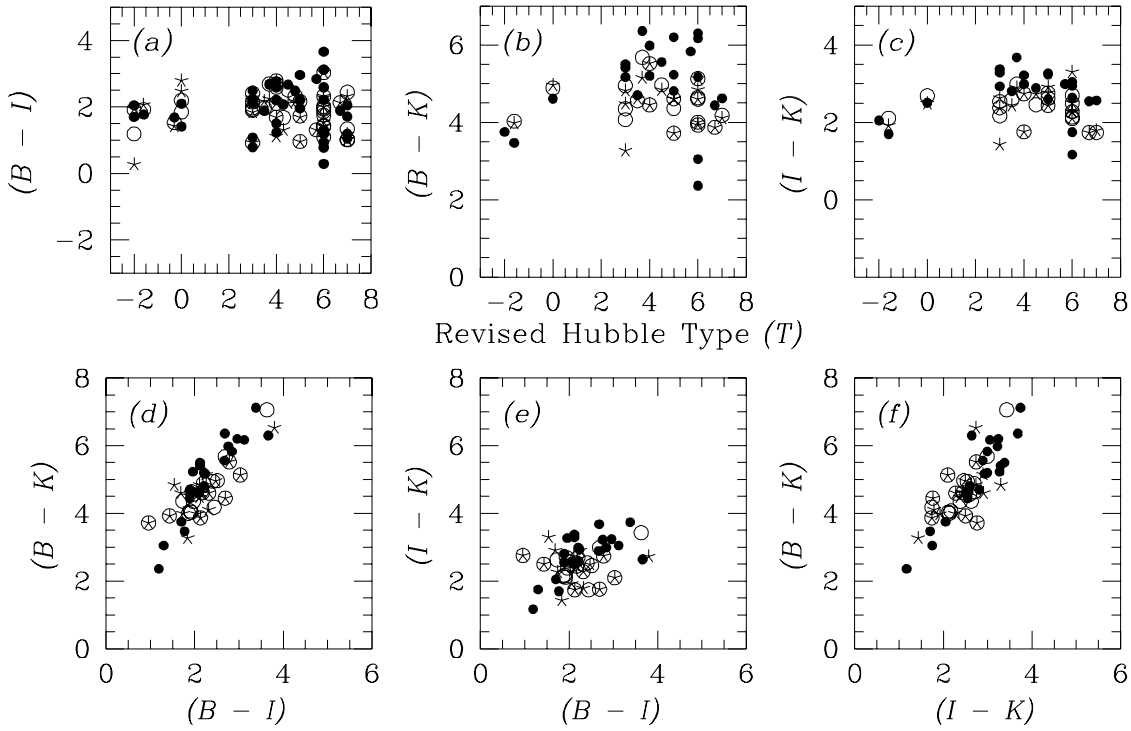

Figure 11. Colour distributions of the sample galaxies: *(a)–(c)* Galaxy colours as a function of revised Hubble type; *(d)–(f)* Colour-colour diagrams. The filled dots denote central galaxy colours (based on the extrapolated central surface brightnesses), the open circles represent the galaxies' total colours, and the stars show the colours of the discs. The galaxy colours have been corrected for Galactic foreground extinction, based on the *(B–V)* colour excesses predicted by Burstein & Heiles (1978, 1984).

gue that the scale height is linearly dependent on the fraction of stellar to gas mass. Under this assumption, it is expected that the vertical scale parameter in the later-type galaxies is smaller than that for the earlier types. However, we cannot confirm this assumption on the basis of our observations.

5.3 Radial colour gradients and extinction

In this paper we show that the mean scale length ratios for the later-type ($T > 2$) disc galaxies in our sample range from $h_I/h_K = 1.15 \pm 0.19$ to $h_B/h_K = 1.65 \pm 0.41$, indicating large colour gradients in the discs. When comparing our results to those published previously we have to keep in mind the nature of our sample: since it consists solely of edge-on disc galaxies, the observed scale length ratios can be expected to be larger than similar ratios obtained from samples including less highly inclined galaxies.

Most previously published scale length ratios favour large colour gradients in galaxy discs:

- For a large sample of face-on galaxies, Elmegreen & Elmegreen (1984) found a mean ratio of $h_B/h_I = 1.16 \pm 0.47$. Using Evans' (1994) models this corresponds to an average ratio of B to K-band scale length of about 1.32.
- Peletier et al. (1994, 1995a) present the results of a study of 37 Sb and Sc galaxies (uniform in orientation on the sky), for which they show that the B to K-band scale length ratio varies between 1.2 and 2, with a mean ratio of $h_B/h_K = 1.49 \pm 0.29$, comparable to our results.
- From de Jong's (1996a) scale length determinations of 86 face-on spiral galaxies, we find an average B to K-band scale length ratio $h_B/h_K = 1.22 \pm 0.23$
- From a study of the prototypical dusty galaxy NGC 253, Forbes & DePoy (1992) find $h_B/h_H = 1.25 \pm 0.05$.

Large colour gradients in galaxy discs between B and I band have also been reported by Kent (1986). However, from a sample of 33 disc galaxies, van der Kruit (1991) reported a small scale length ratio between the photographic J and F bands, $h_J/h_F = 1.07 \pm 0.13$.

The main problem when comparing scale lengths and scale length ratios determined by different authors is the radial fitting range used to derive the scale lengths (Sect. 3.1). However, if scale length ratios are calculated from scale lengths determined over the same radial fitting range in each passband, the differences between different determinations should be $\sim 10\%$ at maximum (Peletier et al. 1994).

Peletier et al. (1994, 1995a,b) argue that scale length ratios due to stellar population changes are of order 1.1–1.2 in the blue – near-infrared range. Two lines of evidence were used to arrive at this result: first, from observations of $T < 1$ type galaxies without much visible dust by Balcells & Peletier (1994), it was found that $h_B/h_I = 1.04 \pm 0.05$, corresponding to B to K-band scale length ratios of at most $h_B/h_K = 1.08 \pm 0.10$, using stellar population models of, e.g., Arimoto & Yoshii (1986). From metallicity gradients from HII regions in galaxy discs, Peletier et al. (1994, 1995a) argue that h_B/h_K is likely of order 1.17, using a simple single-age stellar population model. In the I vs. K range this contribution is likely to be less. Our observations of the scale length ratios in our earliest-type sample galaxies ($T < 1$) support this evidence (Fig. 8).

Therefore, the observed scale length ratios largely represent the galaxies' dust content.

Although the scale length ratios indicate an increasing dust content for galaxy types later than about $T = 3$ (Sb), the data suggests that the distribution of scale length ratios flattens or even decreases towards later types, as was also found from optical depth measurements (e.g., de Grijs et al. 1997). This result is in accordance with the distribution found by Peletier & Balcells (1996).

6 SUMMARY AND CONCLUSIONS

The main conclusions we can draw from the analysis presented in this paper are:

- We found a correlation (although with a large scatter) between the h_R/z_0 ratio and galaxy type, in the sense that galaxies become systematically thinner when going from S0's to Sc's, whereas the later types (Sd's) seem to be at least as thin as the Sc's, but likely thicker.
- The average values found for the h_R/z_0 ratio are significantly smaller than the theoretical prediction of about 10 needed for maximum-disc rotation.
- On average the colour gradients indicated by the scale length ratios increase from type Sa to at least type Scd. For galaxy types later than Scd, the colour gradients seem to become smaller again.
- The observed scale length ratios (and thus the radial colour gradients) largely represent the galaxies' dust content.
- The distribution of (edge-on) K-band disc central surface brightnesses is rather flat, although with a large scatter. However, the latest-type sample galaxies ($T > 6$) show an indication that their disc central surface brightnesses may be fainter than those of the earlier types. Most likely, this effect is not the result of dust extinction.
- We do not find a clear correlation between galaxy type and integrated, disc, or central colours. The scatter in the distributions is probably caused by dust.

Acknowledgements

The input of Reynier Peletier, Piet van der Kruit and Roelof Bottema has been invaluable for the structure and contents of this paper in its present form. This work is based on observations obtained at the European Southern Observatory, La Silla, Chile.

REFERENCES

Aoki, T.E., Hiromoto, N., Takami, H., Okamura, S., 1991, PASJ 43, 755
Arimoto, N., Yoshii, Y., 1986, A&A 107, 135
Balcells, M., Peletier, R.F., 1994, AJ 107, 135
Barnaby, D., Thronson Jr., H.A., 1992, AJ 103, 41
Barteldrees, A., Dettmar, R.-J., 1994, A&AS 103, 475
Bottema, R., 1993, A&A 275, 16
Burstein, D., Heiles, C., 1978, ApJ 225, 40
Burstein, D., Heiles, C., 1984, ApJS 54, 33
Buser, R., 1978, A&A 62, 411

Byun, Y.I., Freeman, K.C., Kylafis, N.D., 1994, ApJ 432, 114
Carlberg, R.G., 1987, ApJ 322, 59
Carter, B.S., Meadows, V.S., 1995, MNRAS 276, 734
Davies, J.I., 1990, MNRAS 244, 8
de Grijs, R., 1997, Ph.D. Thesis, Groningen University
de Grijs, R., Peletier, R.F., 1997, A&A 320, L21
de Grijs, R., Peletier, R.F., van der Kruit, P.C., 1997, A&A 327, 966
de Grijs, R., van der Kruit, P.C., 1996, A&AS 117, 19
de Jong, R.S., 1996a, A&AS 118, 557
de Jong, R.S., 1996b, A&A 313, 45
de Jong, R.S., 1996c, A&A 313, 377
de Jong, R.S., van der Kruit, P.C., 1994, A&AS 106, 451
de Vaucouleurs, G., de Vaucouleurs, A., Corwin, H.G., Jr., Buta, R.J., Paturel, G., Fouqué, P., 1991, Third Reference Catalogue of Bright Galaxies, Springer-Verlag: New York **(RC3)**
Disney, M.J., Davies, J.I., Phillipps, S., 1989, MNRAS 239, 939
Elmegreen, D.M., Elmegreen, B.G., 1984, ApJS 54,127
Evans, R., 1994, MNRAS 266, 511
Fall, S.M., 1983, in: Internal Kinematics and Dynamics of Galaxies, IAU Symposium 100, ed. Athanassoula, E., Dordrecht: Reidel, p. 391
Fall, S.M., Efstathiou, G., 1980, MNRAS 193, 189
Forbes, D.A., DePoy, D.L., 1992, A&A 259, 97
Freeman, K.C., 1970. ApJ 160, 811
Giovanelli, R., Haynes, M.P., Salzer, J.J., Wegner, G., Da Costa, L.N., Freudling, W., 1994, AJ 107, 2036
Guthrie, B.N.G., 1992, A&AS 93, 255
Hamabe, M., Kodaira, K., Okamura, S., Takase, B., 1979, PASJ 31, 431
Hamabe, M., Kodaira, K., Okamura, S., Takase, B., 1980, PASJ 32, 197
Hamabe, M., Wakamatsu, K., 1989, ApJ 339, 783
Hegyi, D.J., Gerber, G., 1979, in: Photometry, Kinematics, and Dynamics of Galaxies, ed. Evans, D.S., Austin: Univ. of Texas Astron. Dept., p. 119
Hubble, E., 1926, ApJ 64, 321
Huizinga, J.E., 1994, Ph.D. Thesis, Groningen University
Jensen, E.B., Thuan, T.X., 1982, ApJS 50, 421
Kent, S.M., 1986, AJ 91, 1301
Kent, S.M., Dame, T.M., Fazio, G., 1991, ApJ 378, 131
Knapen, J.H., van der Kruit, P.C., 1991, A&A 248, 57
Kuchinski, L.E., Terndrup, D.M., 1996, AJ 111, 1073
Kylafis, N.D., Bahcall, J.N., 1987, ApJ 317, 637
Landolt, A.U., 1992, AJ 104, 340
Larson, R.B., Tinsley, B.M., 1978, ApJ 219, 46
Lauberts A., Valentijn, E.A., 1989, The Surface Photometry Catalogue of the ESO-Uppsala Galaxies, ESO **(ESO-LV)**
Mathewson, D.S., Ford, V.L., Buchhorn, M., 1992, ApJS 81, 413
Mathewson, D.S., Ford, V.L., 1996, ApJS 107, 97 (AAS CD-ROM Series, Vol. 7)
Peletier, R.F., 1993, A&A 271, 51
Peletier, R.F., Balcells, M., 1996, in: Spiral Galaxies in the Near-IR, eds. Minnitti, D., Rix, H.-W., ESO/MPA Workshop, p. 48
Peletier, R.F., Balcells, M., 1997, New Astr. 1, 349
Peletier, R.F., Valentijn, E.A., Moorwood, A.F.M., Freudling, W., 1994, A&AS 108, 621
Peletier, R.F., Valentijn, E.A., Moorwood, A.F.M., Freudling, W., 1995a, in: The Opacity of Spiral Disks, ed. Davies, J., NATO Advanced Research Workshop, p. 243
Peletier, R.F., Valentijn, E.A., Moorwood, A.F.M., Freudling, W., Knapen, J.H., Beckman, J.E., 1995b, A&A 300, L1
Peletier, R.F., Willner, S.P., 1992, AJ 103, 1761
Richter, O.-G., Tammann, G.A., Huchtmeier, W.K., 1987, A&A 171, 33
Rieke, G.H., Lebofsky, M.J., 1985, ApJ 288, 618
Sackett, P.D., 1997, ApJ 483, 103
Sandage, A., 1986, A&A 161, 89
Sasaki, T., 1987, PASJ 39, 849
Schmidt, K.-H., Boller, T., 1992, Astron. Nachr. 313, 189
Searle, L., Sargent, W.L.W., Bagnuolo, W.G., 1973, ApJ 179, 427
Shaw, M.A., Gilmore, G., 1990, MNRAS 242, 59
Terndrup, D.M., Davies, R.L., Frogel, J.A., DePoy, D.L., Wells, L.A., 1994, ApJ 432, 518
Thuan, T.X., Gunn, J.E., 1976, PASP 88, 543
Tinsley, B.M., Larson, R.B., 1978, ApJ 221, 554
Toomre, A., 1964, ApJ 139, 1217
van Albada, T.S., Sancisi, R., 1986, Philos. Trans. R. Soc. London, Ser. A 320, 447
van der Kruit, P.C., 1987, A&A 173, 59
van der Kruit, P.C., 1991, in: The World of Galaxies, eds. Corwin, H.G., Bottinelli, L., New York: Springer, p. 256
van der Kruit, P.C., Searle, L., 1981a, A&A 95, 105
van der Kruit, P.C., Searle, L., 1981b, A&A 95, 116
van der Kruit, P.C., Searle, L., 1982a, A&A 110, 61
van der Kruit, P.C., Searle, L., 1982b, A&A 110, 79
Wainscoat, R.J., Freeman, K.C., Hyland, A.R., 1989, ApJ 337, 163
Wainscoat, R.J., Hyland, A.R., Freeman, K.C., 1990, ApJ 348, 85
Wainscoat, R.J., Cowie, L.L., 1992, AJ 103, 332